GLOBAL BIOGEOCHEMICAL CYCLES, VOL. 10, NO. 4, PAGES 809–837, DECEMBER 1996

An improved method for detecting anthropogenic CO_2 in the oceans

Nicolas Gruber

Climate and Environmental Physics, Physics Institute, University of Bern, Bern, Switzerland

Jorge L. Sarmiento

Program in Atmospheric and Oceanic Sciences, Princeton University, Princeton, New Jersey

Thomas F. Stocker

Climate and Environmental Physics, Physics Institute, University of Bern, Bern, Switzerland

Abstract. An improved method has been developed for the separation of the anthropogenic CO_2 from the large natural background variability of dissolved inorganic carbon (C) in the ocean. This technique employs a new quasi-conservative carbon tracer ΔC^*, which reflects the uptake of anthropogenic CO_2 and the air-sea disequilibrium when a water parcel loses contact with the atmosphere. The air-sea disequilibrium component can be discriminated from the anthropogenic signal using either information about the water age or the distribution of ΔC^* in regions not affected by the anthropogenic transient. This technique has been applied to data from the North Atlantic sampled during the Transient Tracers in the Ocean North Atlantic (TTO NAS) and Tropical Atlantic study (TTO TAS) cruises in 1981-1983. The highest anthropogenic CO_2 concentrations and specific inventories (inventory per square meter) are found in the subtropical convergence zone. In the North Atlantic, anthropogenic CO_2 has already invaded deeply into the interior of the ocean, north of 50°N it has even reached the bottom. Only waters below 3000 m and south of 30°N are not yet affected. We estimate an anthropogenic CO_2 inventory of 20 ± 4 Gt C in the North Atlantic between 10°N and 80°N. The 2.5-dimensional ocean circulation model of *Stocker et al.* [1994] and the three-dimensional ocean general circulation biogeochemistry model of *Sarmiento et al.* [1995] predict anthropogenic CO_2 inventories of 18.7 Gt C and 18.4 Gt C, respectively, in good agreement with the observed inventory. Important differences exist on a more regional scale, associated with known deficiencies of the models.

Introduction

It is estimated that the ocean has taken up about 30% (2.0 ± 0.8 Gt C yr^{-1}; 1 Gt = 10^{15} g) of the 7.1 ± 1.1 Gt yr^{-1} released to the atmosphere by human activities in the decade from 1980 to 1989, second in importance only to the accumulation in the atmosphere itself [*Schimel et al.*, 1994]. This estimate is based entirely on indirect methods including observational constraints [*Keeling et al.*, 1989; *Quay et al.*, 1992; *Keeling and Shertz*, 1992; *Enting et al.*, 1995] and ocean models validated mainly with observations of the bomb radiocarbon distribution. Although we firmly support the magnitude of these model estimates [*Sarmiento et al.*, 1992; *Sarmiento and Sundquist*, 1992; *Siegenthaler and Sarmiento*, 1993; *Siegenthaler and Joos*, 1992; *Stocker et al.*, 1994], it must be acknowledged that neither bomb radiocarbon nor the more recently introduced halogenated carbon tracers are ideal tracers of the CO_2 invasion into the oceans. The characteristic air-sea equilibration time of radiocarbon is about an order of magnitude greater than that of CO_2, whereas the equilibration time for freons is about 10 times smaller [*Broecker and Peng*, 1982]. Hence the oceanic inventory of bomb radiocarbon is primarily determined by the air-sea exchange rate, whereas the inventory of anthropogenic CO_2 is controlled by the vertical water transport [*Sarmiento et al.*, 1992; *Siegenthaler and Joos*,

Paper number 96GB01608.
0886-6236/96/96GB-01608$12.00

1992; *Siegenthaler and Sarmiento*, 1993]. Moreover, the temporal evolution of the bomb radiocarbon and freon input into the ocean are very different from that of anthropogenic CO_2. Bomb radiocarbon has been injected in a pulse like manner into the stratosphere in the 1960s with subsequent redistribution into the other carbon reservoirs. The freons, although slowly being stabilized because of their banning, show an increase over time similar to CO_2 but with a much smaller characteristic timescale of about 10 years compared with about 30 to 40 years for anthropogenic CO_2. Until such a time as we are able to pin down the anthropogenic invasion by direct observation, there will always be room for challenges to our estimates of the ocean sink, such as the study of *Tans et al.* [1990] claiming that the oceanic sink for 1980 to 1989 was only 0.3 to 0.8 Gt C yr^{-1}.

Direct determination of the uptake of anthropogenic CO_2 by the oceans can be done following two different strategies (see *Wallace* [1995] for review). One way is by repeated surveys of the carbon system in the ocean that would reveal the increase in concentration over time. However, large variability of the carbon occurs on all timescales because of ocean circulation and seasonal changes in biology and temperature. This variability is comparable in magnitude to the amount of anthropogenic CO_2 and thus obscures the temporal trend of that signal. Furthermore, the high-frequency resampling that is required to get around this problem is difficult to achieve on a large scale. These problems would be largely overcome following the second strategy where a direct estimate of the anthropogenic invasion is attempted. *Brewer* [1978] and *Chen and Millero* [1979] were the first to point out that the anthropogenic CO_2 in the ocean interior can be estimated by correcting the measured C in a water sample for the changes incurred due to the remineralization of organic matter and the dissolution of carbonates since it lost contact with the surface and by subtracting the preformed preindustrial C. Variations of this approach have been pursued by several investigators over the years with varying details [*Chen and Pytkowicz*, 1979; *Chen*, 1982; *Chen*, 1993; *Poisson and Chen*, 1987; *Chen et al.*, 1990; *Chen et al.*, 1995; *Goyet and Brewer*, 1993; *Tsunogai et al.*, 1993].

However, the Brewer and Chen/Millero approach has not found general acceptance, since the uncertainties associated with the estimates were regarded as too large [*Shiller*, 1981; *Shiller*, 1982; *Broecker et al.*, 1985a]. The main points under discussion are the role of mixing of different water types with poorly known initial concentrations, which can lead to nonlinear effects, the difficulty of choosing appropriate preindustrial end-member water types [*Shiller*, 1981], and the large uncertainties in the assumptions relating to the constant stoichiometric ratios and the use of the apparent oxygen utilization (AOU) [*Broecker et al.*, 1985a] for determining the contribution of the remineralization of organic matter.

In this paper, we describe a new technique that eliminates the nonlinear effects due to mixing and which determines the preindustrial C of end-member water types by extrapolation from the distribution of properties in the interior of the ocean. We use water age estimates obtained by tracers to correct the end-member C distribution back to preindustrial times in areas where all interior waters are already contaminated by anthropogenic CO_2. We demonstrate that the contribution of other problems to the final estimates of anthropogenic CO_2 are relatively small (within twice the error of the measurements). The technique is applied to the North Atlantic, where Transient Tracers in the Ocean (TTO) observations of good quality are available. The greatly improved observations presently being obtained by the Joint Global Ocean Flux study (JGOFS) program on World Ocean Circulation Experiment (WOCE) hydrographic sections will soon provide an outstanding opportunity to extend this analysis to the world ocean.

The paper is organized as follows: In the first section we present the new technique employed to separate the anthropogenic CO_2 from the natural background variability. We then describe briefly the data employed in our study and provide an analysis of the error in our estimate of anthropogenic CO_2. Afterward, the results are presented and compared with predictions of two ocean models of different complexity.

Methods

The dissolved inorganic carbon (C) distribution in the ocean is controlled by air-sea gas exchange including the uptake of anthropogenic CO_2 (solubility pump), the biological processes of photosynthesis, respiration, and remineralization (soft-tissue pump), and the formation and dissolution of carbonate particles (carbonate pump) [*Volk and Hoffert*, 1985]. In order to directly quantify the anthropogenic CO_2 from ocean carbon data, a careful technique that accounts for each of these processes must be established. We begin this section with a qualitative description of the approach we follow, using as an example the C data on the sigma theta (σ_θ) 27.0-27.2 surface in the Antarctic Intermediate Water of the Atlantic Ocean. Figure 1a shows the C distribution on this surface plotted versus salinity. The low salinity waters on the left of the diagram originate in the southern hemisphere, whereas the high salinity waters on the right originate in the northern hemisphere. The dominant feature of the data in Figure 1a is the large increase in C concentration in the interior regions due to the influence of the soft-tissue pump and the carbonate pump. We can eliminate the soft tissue contribution by using as an indicator the oxygen concentration; since for each carbon atom added to the deep water because of the remineralization of organic matter, a proportional amount of oxygen is used. The carbonate pump contri-

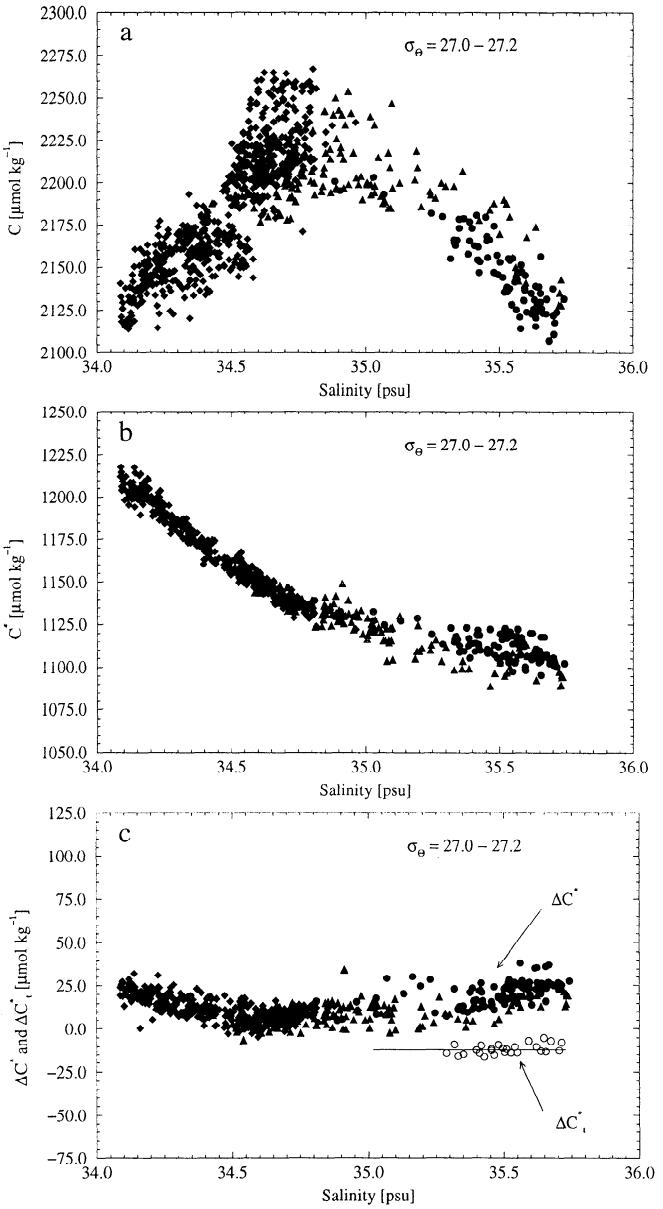

Figure 1. (a) Plot of dissolved inorganic carbon (C) versus salinity in the σ_θ interval 27.0-27.2 in the Atlantic Ocean (Antarctic Intermediate Water). Diamonds denote samples from the South Atlantic Ventilation Experiment (SAVE) cruises, triangles denote samples from the Transient Tracer in the Oceans (TTO) Tropical Atlantic Study (TAS) cruises and circles denote samples from the TTO North Atlantic Study (NAS) cruises. Remineralization of C in the interior of the ocean causes the upward bow. (b) Plot of the conservative tracer C^* versus salinity in the same σ_θ interval. The observations should fall on a straight line, since the internal sources and sinks have been removed. Invasion of anthropogenic CO_2, however, has caused increasing C^* values near the outcrops. (c) Plot of ΔC^* and ΔC_t^* versus salinity in the same σ_θ interval. The amount of anthropogenic CO_2 can be determined by the difference between ΔC^* and ΔC_t^*.

bution is eliminated, using as an indicator the alkalinity distribution corrected for nitrate cycling. These corrections yield the new tracer C^* which is a composite of the preformed oxygen, alkalinity, and preindustrial C concentrations, plus the anthropogenic CO_2 invasion (Figure 1b).

The dominant feature of the C^* distribution is a higher C^* concentration in the southern hemisphere than in the northern hemisphere. The north-south difference of over 100 μmol kg^{-1} is due mainly to the effect of variations in surface salinity and temperature on the solubility of oxygen, with the colder and less salty waters of the southern hemisphere having a greater solubility. We can eliminate most of this trend by correcting C^* for the preformed concentrations using oxygen saturation concentration, surface alkalinity observations, and the preindustrial equilibrium C concentration as a first estimate of preindustrial preformed C. This defines a new tracer ΔC^* (Figure 1c) that reflects the uptake of anthropogenic CO_2 and the air-sea disequilibrium at the time the water lost contact with the atmosphere plus any residual effects due to our choice of oxygen and alkalinity end-members, as well as data and parameter uncertainties. If there were no anthropogenic CO_2 invasion, these data would all fall on a straight line between the southern hemisphere end-member disequilibrium and the northern end-member disequilibrium. One can see an indication of the anthropogenic invasion in the upward trend of ΔC^* as one moves from the interior to the boundaries at either end.

The final task we must achieve in order to identify the anthropogenic CO_2 is to eliminate the air-sea disequilibrium and other residual effects. We make here the assumption that the ocean operates in a steady state and that the CO_2 air-sea disequilibrium has not changed over time. On deeper density surfaces one can use the interior ΔC^* distribution extrapolated to the surface in order to estimate the disequilibrium and residual effects. However, the σ_θ 27.0-27.2 surface has anthropogenic CO_2 at all depths. We therefore use tritium helium–3 ages (available only for the northern hemisphere) to estimate a new tracer ΔC_t^*, calculated relative to the actual atmospheric CO_2 at the time the water parcel left the surface. This gives the lower set of data points at higher salinities in Figure 1c, which show an effective disequilibrium of about −12 μmol kg^{-1}. The difference between ΔC_t^* and ΔC^* is the portion of the original C tracer that can be attributed to the anthropogenic invasion of CO_2. We now describe in more detail the procedures we follow and the assumptions we make in each step of the process that lead to the final analysis in Figure 1. We will also provide an estimate of uncertainty.

Definition of C^*

In the interior of the ocean, away from the surface euphotic layer, the cycling of C is controlled by the remineralization of organic matter and the dissolution of solid calcium carbonates. The latter represents also the main controlling process for alkalinity (Alk). Alk is also affected by the soft-tissue pump due to a proton flux associated with the redox reactions between reduced organic nitrogen and nitrate [*Brewer et al.*, 1975]. The magnitude of this proton flux has been called into question by *Shiller and Gieskes* [1980] and *Shiller* [1981] but seems to be well established today [*Broecker and Peng*, 1982; *Goyet and Brewer*, 1993]. By contrast, the biogeochemical cycling of oxygen is entirely governed by the soft-tissue pump. The tracer continuity equation for C, Alk, and O_2 in the interior of the ocean can therefore be written as

$$\Gamma(C) = J_{\text{soft}}(C) + J_{\text{carb}}(C), \quad (1)$$

$$\Gamma(Alk) = J_{\text{soft}}(Alk) + J_{\text{carb}}(Alk), \quad (2)$$

$$\Gamma(O_2) = J_{\text{soft}}(O_2), \quad (3)$$

where J_{soft} denotes the source minus sink term due to the remineralization of organic matter and J_{carb} denotes the source minus sink term due to the dissolution of solid calcium carbonates. The operator Γ represents the transport and time rate of change:

$$\Gamma(T) = \frac{\partial T}{\partial t} + \vec{u} \cdot \nabla T - \nabla \cdot (D \cdot \nabla T), \quad (4)$$

where T represents any tracer concentration, ∇ represents the gradient operator in three – dimensions, $\vec{u}$ represents the velocity field, and D represents the eddy diffusivity tensor.

We assume that the soft-tissue pump influences C and O_2 with a constant stoichiometric ratio ($r_{C:O_2}$) and that the carbonate pump changes alkalinity twice as much as it changes C. The proton flux during the processes of photosynthesis, respiration, and remineralization is assumed to be proportional to the change in the nitrate concentration, which in turn is proportional to the change in O_2 through the constant stoichiometric ratio $r_{N:O_2}$ thus

$$J_{\text{soft}}(C) = r_{C:O_2} J_{\text{soft}}(O_2), \quad (5)$$

$$J_{\text{carb}}(C) = \tfrac{1}{2} J_{\text{carb}}(Alk), \quad (6)$$

$$J_{\text{soft}}(Alk) = -J_{\text{soft}}(NO_3) = -r_{N:O_2} J_{\text{soft}}(O_2). \quad (7)$$

Substituting these relationships (equations (5) - (7)) into (1) and (2) gives

$$\Gamma(C) = r_{C:O_2} J_{\text{soft}}(O_2) + \tfrac{1}{2} J_{\text{carb}}(Alk), \quad (8)$$

$$\Gamma(Alk) = -r_{N:O_2} J_{\text{soft}}(O_2) + J_{\text{carb}}(Alk). \quad (9)$$

We can eliminate the J_{soft} and J_{carb} terms from the C equation (8) by subtracting $r_{C:O_2}\Gamma(O_2)$ and $\frac{1}{2}(\Gamma(Alk) + r_{N:O_2}\Gamma(O_2))$ from it:

$$\Gamma(C) - r_{C:O_2}\Gamma(O_2) - \tfrac{1}{2}\left(\Gamma(Alk) + r_{N:O_2}\Gamma(O_2)\right) = 0. \quad (10)$$

Since we assumed constant stoichiometric ratios ($r_{C:O_2}$ and $r_{N:O_2}$, respectively), the C, Alk, and O_2 equations are linear, and therefore the transport and time rate of change operators Γ can be combined to $\Gamma(C - r_{C:O_2}O_2 - \frac{1}{2}(Alk + r_{N:O_2}O_2))$. This permits us to define a new tracer C^*,

$$C^* = C - r_{C:O_2}O_2 - \tfrac{1}{2}\left(Alk + r_{N:O_2}O_2\right), \quad (11)$$

with conservative properties

$$\Gamma(C^*) = 0. \quad (12)$$

The distribution of C^* is strongly influenced by the preformed concentrations of C, Alk, and O_2 and reflects therefore, similar to Broecker's conservative water mass tracer PO [*Broecker*, 1974], mostly differences in the origin of the different water masses (see Figure 1).

Definition of ΔC^*

We can eliminate most of the influence of the origins of the different water masses by only considering deviations of C^* from its preindustrial preformed value C^{*0} and denoting this new quantity by ΔC^*:

$$\Delta C^* = C^* - C^{*0}, \quad (13)$$

$$C^{*0} = C^0 - r_{C:O_2}O_2^0 - \tfrac{1}{2}\left(Alk^0 + r_{N:O_2}O_2^0\right), \quad (14)$$

where the superscript zero denotes preformed concentrations. We estimate the preindustrial preformed concentration of C (C^0) by the equilibrium C concentration (C_{eq}) for a preindustrial atmospheric CO_2 fugacity of 280 μatm [*Neftel et al.*, 1994] thereby neglecting for the moment the fact that surface C is seldom in equilibrium with the atmospheric CO_2 fugacity. Preformed O_2 (O_2^0) is estimated by its saturation concentration O_2^{sat} and preformed Alk (Alk^0) by a multiple linear regression (see appendix A). We wish to maintain the conservative properties of ΔC^*. This requires linearizing the C_{eq} and O_2^{sat} equations. Appendix A shows how we linearize C_{eq}. For O_2^{sat} we assume that the nonlinear effects on a given density surface are negligible compared to other uncertainties. We thus have

$$\Delta C^* = C - C_{\text{eq}}(S, T, Alk^0)\,|_{fCO_2 = 280\ \mu\text{atm}} - r_{C:O_2}\left(O_2 - O_2^{\text{sat}}\right) - \tfrac{1}{2}\left(Alk - Alk^0 + r_{N:O_2}\left(O_2 - O_2^{\text{sat}}\right)\right), \quad (15)$$

$$\Gamma\left(\Delta C^*\right) \approx 0. \quad (16)$$

The variability of ΔC^* reflects then only the ocean uptake of anthropogenic CO_2 and the CO_2 air-sea disequilibrium at the time the water lost contact with the atmosphere plus any residual effects due to our choice of end-members and data uncertainties. The determination of the preformed values in (15) and its uncertainties are described in detail in appendix A.

We use the stoichiometric ratios determined by *Anderson and Sarmiento* [1994] throughout our study. By using a nonlinear inverse method on neutral surfaces, they found that these ratios are $P : N : C_{org} : O_2 = 1 : 16 \pm 1 : 117 \pm 14 : -170 \pm 10$ and approximately independent of depth and ocean basin. These stoichiometric ratios have been the subject of an intense scientific debate over recent years, and several modifications have been proposed to the "traditional" $P : N : C_{org} : O_2$ stoichiometric ratios of *Redfield et al.* [1963] (1 : 16 : 103 : −138). *Takahashi et al.* [1985a], *Broecker et al.* [1985b], and *Peng and Broecker* [1987] concluded in their studies that the $O_2 : P$ ratio is significantly higher at −172 and −175, respectively, and that this ratio is nearly constant at all depths throughout the entire ocean. In conflict with this, *Minster and Boulahdid* [1987] and *Boulahdid and Minster* [1989] suggested that the $O_2 : P$ ratio, while near −172 in the thermocline, decreases in depth to approximately −115 in all oceans. The study of *Anderson and Sarmiento* [1994], which encompasses all previous ones with regard to data coverage and treatment of the mixing problem, generally confirms the results of *Takahashi et al.* [1985a] and *Broecker et al.* [1985b]. We therefore consider the proposed ratios of *Anderson and Sarmiento* [1994] to be the best ones currently available.

Calculating the Anthropogenic CO_2

Since the variability of ΔC^* is due to the uptake of anthropogenic CO_2 and the air-sea disequilibrium of CO_2 when a water parcel was last in contact with the atmosphere plus any residual effects of our choice of oxygen and alkalinity end-members, we must eliminate the total "effective" disequilibrium effect from ΔC^*, to obtain a purely anthropogenic signal. The assumptions are made that the ocean has been operating in a steady state, that the effective disequilibrium has stayed more or less constant within the outcrop region of a particular isopycnal surface, and that the water transport is predominantly along isopycnal surfaces. If these assumptions are correct, the concentration of ΔC^* on a isopycnal surface should reveal the history of the CO_2 uptake (see Figure 1). We will determine the effective air-sea equilibrium for the outcrops of 28 isopycnal surfaces in the North Atlantic and then use a smoothing spline to represent this disequilibrium as a function of the density of the seawater, $\Delta C_{\text{dis eq}}(\rho)$.

The amount of anthropogenic CO_2 in the ocean (ΔC_{ant}) can finally be calculated by

$$\Delta C_{\text{ant}} = \Delta C^* - \Delta C_{\text{dis eq}}(\rho). \tag{17}$$

In the next section we describe in detail how the CO_2 air-sea disequilibrium can be estimated from ΔC^* and information about the apparent age of a water parcel.

Determining the Effective Air-Sea Disequilibrium

We determine the effective disequilibrium as a function of the potential density of a water parcel using two different methods.

ΔC^* method. In the first method we look at the variability of ΔC^* on deep ocean density surfaces in regions far away from the outcrop, where one can safely assume that there is no anthropogenic CO_2 contamination. ΔC^* in these uncontaminated regions reflects therefore a mixture of the effective air-sea disequilibria of the different end-member water masses. It turns out, in all the cases we consider in the deep North Atlantic and tropical Atlantic, that ΔC^* in the uncontaminated regions does not show a significant trend with amount of southern and northern end-member water mass (determined from PO_4^* [*Broecker et al.*, 1991]). We therefore neglect this potential complication and calculate the effective air-sea disequilibrium as if all water has a single end-member water mass,

$$\Delta C_{\text{dis eq}} = \overline{\Delta C^*}\big|_{\sigma=\text{const}}, \tag{18}$$

where $\overline{\Delta C^*}\big|_{\sigma=\text{const}}$ represents the mean ΔC^* of the isopycnal surface interval in the region without anthropogenic influence.

The ΔC^* method does not work, however, for shallow isopycnal surfaces since anthropogenic CO_2 has already affected the entire surface, and therefore no region without anthropogenic CO_2 can be found. It also fails for surfaces in the Greenland and Norwegian Seas (density surfaces greater than $\sigma_\theta = 27.90$) because here anthropogenic CO_2 has also penetrated into the whole water column, as is evident from the presence of bomb tritium [*Schlosser et al.*, 1995]. We therefore use the first method only for all surfaces denser than $\sigma_2 = 36.95$ (average depth 2000 m) with the exception of the water masses in the Greenland and Norwegian Seas.

ΔC_t^* method. For shallower surfaces and the waters in the Greenland and Norwegian Seas we employ a second method to determine $\Delta C_{\text{dis eq}}$. If the age of a water parcel is known, the C concentration in equilibrium with the atmospheric CO_2 for the time when the water parcel left the surface ($C_{\text{eq}}(t)$) can be calculated. Subtracting $C_{\text{eq}}(t)$ instead of C_{eq} in (15) gives ΔC_t^*:

$$\begin{aligned}\Delta C_t^* = {} & C - C_{\text{eq}}(S, T, Alk^0, fCO_2(t_{\text{sample}} - \tau)) \\ & - r_{C:O_2}\left(O_2 - O_2^{\text{sat}}\right) \\ & - \tfrac{1}{2}\left(Alk - Alk^0 + r_{N:O_2}\left(O_2 - O_2^{\text{sat}}\right)\right),\end{aligned} \tag{19}$$

where $fCO_2(t_{\text{sample}} - \tau)$ denotes the atmospheric CO_2 fugacity at the moment when the water parcel was last in contact with the atmosphere. This date is calculated by subtracting the water age τ from the sampling date, t_{sample}. This substitution removes the anthropogenic CO_2 signal from ΔC^* but does not correct for residual effects due to our choice of oxygen and alkalinity endmembers. However, we argue in appendix A that these residual effects should be relatively small. As on deeper surfaces, we find that ΔC_t^* is constant within the uncertainty, implying that the different source regions for this water mass have very nearly the same air-sea disequilibrium. The effective air-sea disequilibrium $\Delta C_{\text{dis eq}}$ is thus determined by

$$\Delta C_{\text{dis eq}} = \overline{\Delta C_t^*}\big|_{\sigma=\text{const}}, \tag{20}$$

where $\overline{\Delta C_t^*}\big|_{\sigma=\text{const}}$ is the mean ΔC_t^* on the density surface under consideration.

It should be possible to use any tracer or tracer combination that contains water age information (CFC 11/CFC 12, $^{228}Ra/^{226}Ra$ and tritium helium–3) to determine $C_{\text{eq}}(t)$. We use concurrent tritium (^3H) and helium–3 (^3He) measurements to calculate the tritium helium–3 age ($\tau_{T/He}$) following the method of *Jenkins* [1987]:

$$\tau_{T/He} = \lambda^{-1} \cdot \ln\left(1 + \frac{[^3He]}{[^3H]}\right), \tag{21}$$

where the brackets denote the concentrations in appropriate units (tritium units) and λ is the tritium decay constant ($1.77 \cdot 10^{-9}$ s^{-1}).

We are able to determine the ^3H-^3He age and ΔC_t^* for the North Atlantic north of 15°N only, since we have tritium and helium observations available only from the transient tracer in the ocean North Atlantic Study (TTO NAS, 1980). These data were obtained by the Woods Hole Oceanographic Institution Helium Isotope Laboratory headed by W. J. Jenkins. The atmospheric CO_2 fugacity at the time the water left the surface ($t_{\text{sample}} - \tau_{T/He}$) was estimated from a smoothing spline fit through atmospheric CO_2 data obtained from direct observations after 1958 [*Keeling and Whorf*, 1994] and ice-core data before 1958 [*Neftel et al.*, 1994].

The ΔC_t^* method to determine the air-sea disequilibrium would also permit a shortcut for determining the anthropogenic CO_2 directly. Replacing the mean ΔC_t^* along an isopycnal surface in (20) by the individual ΔC_t^* values and inserting the resulting expression for $\Delta C_{\text{dis eq}}$ into (17) for ΔC_{ant} yields

$$\Delta C_{\text{ant}} = C_{\text{eq}}(S, T, Alk^0, fCO_2(t_{\text{sample}} - \tau)) - C_{\text{eq}}(S, T, Alk^0)\,|_{fCO_2 = 280\ \mu\text{atm}}. \tag{22}$$

Thus all that is necessary to determine anthropogenic CO_2 in the ocean is an exact knowledge of the water age and measurements of the standard hydrographic parameters, for example, temperature, salinity, phosphate, and oxygen. However, we did not make use of this shortcut for two reasons. First, there are almost an order of magnitude fewer observations available for tritium and helium–3 in comparison to carbon thereby reducing the number of estimates for anthropogenic CO_2 by that amount. Second, the uncertainties with regard to the water age would enter directly into the estimate of anthropogenic CO_2, without control over whether the assumptions behind this shortcut are reasonable or not.

Caveats. Although many of the assumptions we make to determine $\Delta C_{\text{dis eq}}$ are problematic and have large uncertainties (e.g., constant air-sea disequilibrium, etc.), the feasibility of them can be tested with the observational results, and it turns out this test generally confirms the assumptions. However, there are two caveats that need further discussion. The first caveat concerns the assumption of a constant air-sea disequilibrium over time, and the second is related to the estimate of the water age.

Regarding the first major caveat, we must take into consideration that the global mean CO_2 air-sea disequilibrium has not stayed constant, since the ocean is lagging behind the atmospheric anthropogenic CO_2 increase. The global mean anthropogenic air-sea disequilibrium required to sustain the present global anthropogenic CO_2 uptake of about 2 Gt C yr^{-1} is of the order of 8 μatm [*Siegenthaler and Sarmiento*, 1993]. Such a ΔfCO_2 of about 8 μatm corresponds to an air-sea disequilibrium of about 5 μmol kg^{-1} in C. It should be possible, in principle, to detect this trend in the data and to correct for it. However, the uncertainties in the data and parameters we use give a ΔC^* uncertainty of 9 μmol kg^{-1}, which is too large to see this trend.

For the determination of ΔC_t^* we must consider that the ^3H-^3He age is not equal to the true water age. Mixing affects the ^3H-^3He age in a nonlinear way by making it younger compared to the "true" water age [*Jenkins*, 1987]. *Thiele and Sarmiento* [1990] investigated the difference between the true and the ^3H-^3He age along isopycnals and found that the difference is strongly influenced by the the water age and by the relative importance of advection and diffusion. For waters younger than a decade the difference is only important if diffusion is the dominant transport process along these isopycnal surfaces. However, for most areas of the ocean, advection is thought to be controlling the transport, and we therefore neglect the difference between the true and the ^3H-^3He age.

Isopycnal Surfaces. We determined $\Delta C_{\text{dis eq}}$ on a total of 28 isopycnal surfaces in the North Atlantic. For the thermocline and the middepth waters we chose more or less the same surfaces as *Kawase and Sarmiento* [1985] and *Kawase and Sarmiento* [1986] and augmented them with additional isopycnal layers near the surface,

Table 1. Potential Density Surfaces Used in This Study

Potential Density		Depth, m [a]	Description	Water Masses [b]
Midvalue	Interval			
		σ_θ Surfaces		
25.30	25.00 - 25.45	50-100		
25.60	25.45 - 25.75	50-150	salinity maximum oxygen maximum	Subtropical Underwater
25.90	25.75 - 26.05			
26.20	26.05 - 26.35	100-200		
26.50	26.35 - 26.65	150-400		18° Water
26.80	26.65 - 26.95	200-700		
27.10	26.95 - 27.25	450-900		Subpolar Mode Water
27.30	27.25 - 27.35		salinity minimum	Antarctic Intermediate
27.40	27.35 - 27.45	700-1050	salinity minimum	Antarctic Intermediate
		σ_2 Surfaces		
36.45	36.40 - 36.50	800 - 1100	salinity minimum	Antarctic Intermediate
36.55	36.50 - 36.60	1100 - 1150	salinity maximum	Mediterranean Outflow
36.65	36.60 - 36.70	1150 - 1200	salinity maximum	Mediterranean Outflow
36.75	36.70 - 36.80	1200 - 1500	salinity maximum (eastern basin)	Mediterranean Outflow
36.85	36.80 - 36.90	1500 - 1600	silica maximum salinity maximum (western basin)	Labrador Sea, Upper NADW
36.95	36.90 - 36.98	1950 - 2350	oxygen maximum	middle NADW, DSOW, ISOW
37.00	36.98 - 37.03	2300 - 2800	oxygen maximum	middle NADW, DSOW, ISOW
37.05	37.03 - 37.08	2950 - 3300		DSOW, ISOW
		σ_4 Surfaces		
45.825	45.813 - 45.838	3200 - 3400	oxygen minimum nutrient maximum	
45.850	45.838 - 45.863	3500 - 3800		lower NADW
45.875	45.863 - 45.888	3800 - 3900	oxygen maximum nutrient minimum	lower NADW (ISOW,DSOW)
45.900	45.888 - 45.913	4500 - 4700		(western basin only)
45.925	45.913 - 45.938	5000 - 5500	low salinity low oxygen	Antarctic Bottom (western basin only)
45.950	45.938 - 45.963	5500 - 6000		(western basin only)
		σ_θ Surfaces in the Greenland and Norwegian Seas		
27.92	27.90 - 27.94			
27.96	27.94 - 27.98			
28.00	27.98 - 28.02			
28.04	28.02 - 28.06			
28.08	28.06 - 28.10			

[a]Depth range of the surface south of the steeply sloping region leading to the outcrop.
[b]NADW, North Atlantic Deep Water; LSW, Labrador Sea Water; DSOW, Denmark Strait Overflow Water; ISOW, Iceland-Scotland Overflow Water.

in the deep ocean and in the Greenland and Norwegian Seas. A summary of the chosen surfaces and their characteristics is given in Table 1. For the analysis of $\Delta C_{\text{dis eq}}$ we excluded observations above 100 m depth, since our approach is limited to waters below the euphotic layer, which is on average about 50 to 100 m deep. We furthermore removed all stations lying poleward of the wintertime outcrops as determined from the National Oceanic and Atmospheric Administration (NOAA) Atlas [*Levitus et al.*, 1994; *Levitus and Boyer*,

1994]. To obtain a continuous numerical representation of $\Delta C_{\text{dis eq}}$ as a function of density, $\Delta C_{\text{dis eq}}(\rho)$, a smoothing spline function is applied to the results from the 28 density surfaces.

Data Considerations

We use C, Alk, O_2, and nutrient data from the Geochemical Ocean Section Study (GEOSECS) program (1972–1978) [*Bainbridge*, 1981a; *Broecker et al.*, 1982; *Weiss et al.*, 1983], the Transient Tracers in the Ocean North Atlantic Study (TTO NAS) program (1981) [*PCODF*, 1986a; *Brewer et al.*, 1986], the Transient Tracers in the Ocean Tropical Atlantic Study (TTO TAS) program (1982–1983) [*PCODF*, 1986b] and the South Atlantic Ventilation Experiment (SAVE) program (1987–1989) [*ODF*, 1992a; *ODF*, 1992b, Takahashi, personal communication, 1995]. The station locations of the cruises in the Atlantic are shown in Figure 2. We use the revised version of the TTO NAS C data, recalculated from fCO_2 and Alk by *Takahashi and Brewer* [1986], after a systematic discrepancy was discovered between the original C data and the measurements of the Carbon Dioxide Research Group (CDRG) at the Scripps Institution of Oceanography [*Bradshaw and Brewer*, 1988]. The C and Alk data have been measured by many different methods and therefore have variable precision and accuracy as discussed in detail in appendix B.

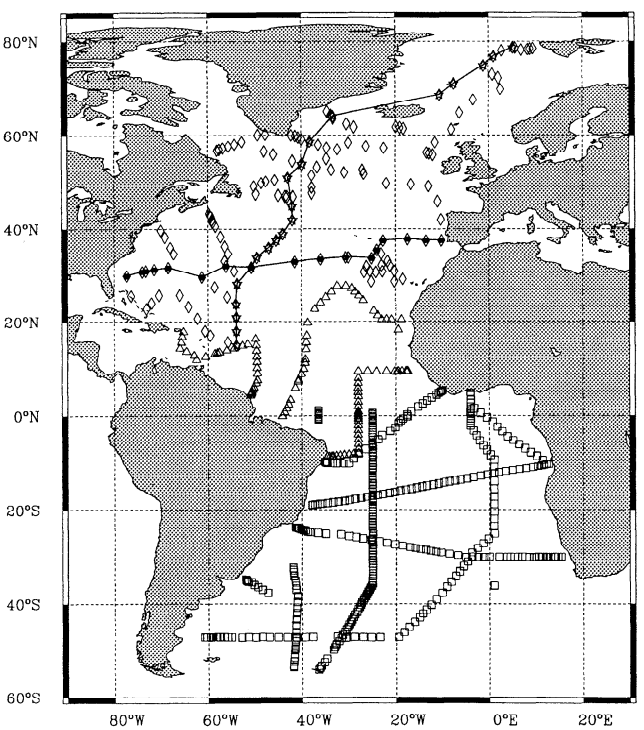

Figure 2. Hydrographic station locations of the TTO North Atlantic Study (TTO NAS, 1981)(diamonds), TTO Tropical Atlantic Study (TTO TAS, 1982/1983) (triangles), and the South Atlantic Ventilation Experiment (SAVE, 1988/1989)(squares). The tracks of the sections used in later illustrations are shown as lines.

For ΔC^* to be a useful conservative tracer and for getting a high quality estimate of the amount of anthropogenic CO_2 in the ocean, it is necessary to insure the internal consistency of the C and Alk data sets. This consistency check has already been done for the GEOSECS data set (*Broecker et al.* [1985] and others), and we therefore applied the proposed corrections as summarized by *Anderson and Sarmiento* [1994] (see appendix B). We investigated the internal consistency of the more modern Atlantic data by looking at deep ocean (> 3500 m) C and Alk trends versus temperature in 10° latitude by 10° longitude areas which have been repeatedly sampled by different legs or cruises. Systematic offsets between the different legs and cruises have been found and corrected as described in detail in appendix B. Possible inaccuracies of the Atlantic carbon data were assessed by comparing them with the shore-based C and Alk measurements obtained by the Carbon Dioxide Research Group at the Scripps Institution of Oceanography (C.D. Keeling, personal communication, 1994). This comparison showed good agreement within the precision of the measurements (see appendix B).

The data in the Atlantic Ocean have been sampled over a period of 8 years. During this period, atmospheric CO_2 rose from approximately 340 μatm in 1981 to 353 μatm in 1989 [*Keeling and Whorf*, 1994]. Temporal variability has been assessed by comparing reoccupied and closely revisited stations between the TTO NAS, TTO TAS, and SAVE cruises. This analysis revealed mostly no significant changes in water mass characteristics, although such changes have been reported by *Brewer et al.* [1983], *Broecker* [1985], and *Swift* [1984b] for the preceding decade between 1972 and 1982 for the water masses south of Greenland. This variability seems to be restricted to the northern North Atlantic, where we only make use of the TTO NAS data set. In the overlapping regions of the different cruises, no such changes have been reported. We therefore neglect possible existing temporal variability in our data sets and combine all data as if they were synoptic.

Error Assessment

Analysis of the variability of ΔC^* requires assessment of the errors due to uncertainties in the stoichiometric ratios ($\sigma_{r_{C:O_2}}$ and $\sigma_{r_{N:O_2}}$), the determination of preformed Alk (σ_{Alk}), the linearized C_{eq} ($\sigma_{C_{\text{eq}}}$), the errors during tracer sampling and measurement (σ_C, σ_{Alk}, and σ_{O_2}), and the uncertainty due to a possible oxygen disequilibrium between the ocean and the atmosphere

($\sigma_{O_2^{sat}}$). We assume for the moment that systematic errors are relatively small and partially accounted for by our technique for finding ΔC_{ant}. We neglect the very small errors in temperature and salinity sampling and analysis. We assume that the analytical determinations of the tracers and the stoichiometric ratios are unrelated and that therefore the associated errors are independent and uncorrelated. The error of ΔC^* ($\sigma_{\Delta C^*}$) is then given by

$$\sigma^2_{\Delta C^*} = \left\{\frac{\partial \Delta C^*}{\partial C}\sigma_C\right\}^2 + \left\{\frac{\partial \Delta C^*}{\partial C_{eq}}\sigma_{C_{eq}}\right\}^2 + \left\{\frac{\partial \Delta C^*}{\partial r_{C:O_2}}\sigma_{r_{C:O_2}}\right\}^2 + \left\{\frac{\partial \Delta C^*}{\partial O_2}\sigma_{O_2}\right\}^2 + \left\{\frac{\partial \Delta C^*}{\partial O_2^{sat}}\sigma_{O_2^{sat}}\right\}^2 + \left\{\frac{\partial \Delta C^*}{\partial Alk}\sigma_{Alk}\right\}^2 + \left\{\frac{\partial \Delta C^*}{\partial Alk^0}\sigma_{Alk^0}\right\}^2 + \left\{\frac{\partial \Delta C^*}{\partial r_{N:O_2}}\sigma_{r_{N:O_2}}\right\}^2 \quad (23)$$

$$\sigma^2_{\Delta C^*} = \{\sigma_C\}^2 + \{-\sigma_{C_{eq}}\}^2 + \left\{-\left(O_2 - O_2^{sat}\right)\sigma_{r_{C:O_2}}\right\}^2 + \left\{\left(-r_{C:O_2} - \tfrac{1}{2}r_{N:O_2}\right)\sigma_{O_2}\right\}^2 + \left\{\left(r_{C:O_2} + \tfrac{1}{2}r_{N:O_2}\right)\sigma_{O_2^{sat}}\right\}^2 + \left\{-\tfrac{1}{2}\sigma_{Alk}\right\}^2 + \left\{\left(-\frac{\partial C_{eq}}{\partial Alk} + \tfrac{1}{2}\right)\sigma_{Alk^0}\right\}^2 + \left\{-\tfrac{1}{2}\left(O_2 - O_2^{sat}\right)\sigma_{r_{N:O_2}}\right\}^2. \quad (24)$$

The error of ΔC^* is therefore dependent on AOU (O_2^{sat} - O_2). Figure 3 shows a plot of $\sigma_{\Delta C^*}$ versus AOU based on the following error estimates: $\sigma_C = 5$ μmol kg^{-1}; $\sigma_{C_{eq}} = 4$ μmol kg^{-1}; $\sigma_{r_{C:O_2}} = 0.092$; $\sigma_{O_2} = 1$ μmol kg^{-1}; $\sigma_{O_2^{sat}} = 4$ μmol kg^{-1}; $\sigma_{Alk} = 5$ μeq kg^{-1}; $\sigma_{Alk^0} = 11$ μeq kg^{-1}; and $\sigma_{r_{N:O_2}} = 0.0081$. The estimated uncertainties of the measurements and the preformed values are discussed in detail in the appendices. The uncertainties of the stoichiometric ratios, $\sigma_{r_{C:O_2}}$ and $\sigma_{r_{N:O_2}}$, have been determined by error propagation of the uncertainties given by *Anderson and Sarmiento* [1994].

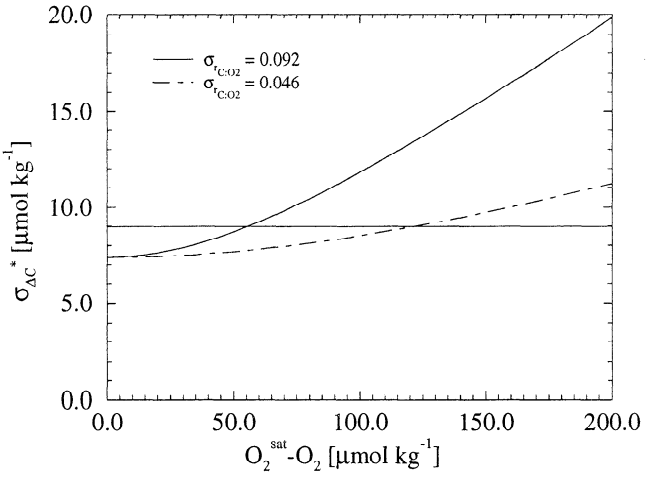

Figure 3. Estimated error of ΔC^*, $\sigma_{\Delta C^*}$ plotted versus AOU ($O_2^{sat} - O_2$) for two values of the error of $\sigma_{r_{C:O_2}}$. The line at $\sigma_{\Delta C^*} = 9$ μmol kg^{-1} denotes our chosen uncertainty for ΔC^*.

Table 2 shows the relative contribution of the various terms in (24) (relative to the square of the total error, e.g., $\sigma^2_{\Delta C^*}$). The error due to σ_{O_2}, $\sigma_{O_2^{sat}}$, and $\sigma_{r_{N:O_2}}$ is always negligible. The other terms, except for the error due to $\sigma_{r_{C:O_2}}$, are all of the same order and lead to an error of 7.9 μmol kg^{-1} for zero AOU. The error due to uncertainties in the $C : O_2$ stoichiometric ratio, $\sigma_{r_{C:O_2}}$, becomes significant only for AOU greater than 80 μmol kg^{-1}. Since most anthropogenic CO_2 will be found in waters with relatively low AOU, we estimate for ΔC^* an error of the order of 9 μmol kg^{-1} (equal to the error for an AOU of 50 μmol kg^{-1}).

The uncertainty of the amount of anthropogenic CO_2 in the ocean, $\sigma_{\Delta C_{ant}}$, is estimated by quadratic error addition of the error in ΔC^* ($\sigma_{\Delta C^*}$) and $\Delta C_{\text{dis eq}}$ ($\sigma_{\Delta_{dis\,eq}}$). We estimated the latter to be about $\pm$ 4 μmol kg^{-1} by taking the average $\sigma_{\Delta C_{dis\,eq}}$ value of all density surfaces (see Table 3). This gives an uncertainty of $\pm$10 μmol kg^{-1} for ΔC_{ant}. The anthropogenic C content of the ocean ranges from 0 to about 50 μmol kg^{-1}. The signal to noise (error) ratio of ΔC_{ant} is therefore ≈ 5.

Table 2. Relative Error Contribution to ΔC^*

AOU, μmol kg^{-1}	$\sigma_{\Delta C^*}$, μmol kg^{-1}	σ_C, %	$\sigma_{C_{eq}}$, %	$\sigma_{r_{C:O_2}}$, %	σ_{O_2}, %	$\sigma_{O_2^{sat}}$, %	σ_{Alk}, %	σ_{Alk^0}, %	$\sigma_{r_{N:O_2}}$, %
0	7.9	40	26	0	0	0	10	23	0
50	9.1	30	19	26	0	0	8	17	0
100	12.1	17	11	58	0	0	4	10	0
150	15.9	9	6	75	0	0	3	6	0
200	20.0	6	4	84	0	0	2	4	0

Error contribution is based on (24) for $\sigma_C = 5$ μmol kg^{-1}; $\sigma_{C_{eq}} = 4$ μmol kg^{-1}; $\sigma_{r_{C:O_2}} = 0.092$; $\sigma_{O_2} = 1$ μmol kg^{-1}; $\sigma_{O_2^{sat}} = 4$ μmol kg^{-1}; $\sigma_{Alk} = 5$ μeq kg^{-1}; $\sigma_{Alk^0} = 11$ μeq kg^{-1} and $\sigma_{r_{N:O_2}} = 0.0081$.

It was assumed above, for estimating the uncertainty of ΔC^* and ΔC_{ant}, that all errors are random and independent. However, some of the errors might be of systematic origin. We show in the appendices that these systematic errors are small for the use of the oxygen saturation concentration for preformed oxygen, for preformed alkalinity, as well as for inaccuracies in the determination of C and Alk. Even if these systematic errors are larger, they do not affect our anthropogenic CO_2 results, since ΔC_{ant} is calculated by difference of the two quantities ΔC^* and $\Delta C_{\text{dis eq}}$, which are equally affected by a systematic offset (see (17)) in these quantities.

With the reported precision of the modern coulometric C and titrimetric Alk data of ± 1 μmol kg^{-1} and ± 2 μeq kg^{-1}, respectively [*Millero*, 1995, Table 1], the error of ΔC^* for zero AOU is lowered to 5 μmol kg^{-1}, with the largest contribution coming from σ_{Alk^0} and $\sigma_{C_{eq}}$. The influence of the uncertainty in the $C : O_2$ stoichiometric ratio, $\sigma_{r_{C:O_2}}$, starts to dominate $\sigma_{\Delta C^*}$ for AOU greater than 45 μmol kg^{-1}. This implies that the uncertainty of ΔC_{ant} is ultimately limited by the uncertainty of this stoichiometric ratio.

Results and Discussion

ΔC^* and ΔC_t^*

Figure 4 shows ΔC^* as a function of latitude for 2 of the 10 deep isopycnal surfaces where we determined the air-sea disequilibrium by the first ΔC^* method. These surfaces are the σ_2 interval 36.98–37.03 which is the core of the middle North Atlantic Deep Water (NADW) (average depth 2500 m) and the σ_4 interval 45.888–45.913 (average depth 4500 m) which represents the boundary between the Antarctic Bottom Water and the lower NADW. ΔC^* near the outcrop regions of these deep surfaces in the north and south shows increasing values due to the uptake of anthropogenic CO_2. The ΔC^* away from the outcrops is remarkably uniform within the uncertainty of ΔC^*. This supports our assumption that the effective CO_2 disequilibrium has stayed more or less constant over time. It furthermore shows that effective air-sea disequilibrium in the northern and southern outcrop region is very nearly the same. We chose the region from 20°S to 20°N as the region without anthropogenic CO_2 to determine $\Delta C_{\text{dis eq}}$. Limited information on water ages in that region from ^{39}Ar analysis [*Rodriguez*, 1993] confirm that most of these waters are older than 150 years. *Weiss et al.* [1985] showed, however, that CCl_3F originating from the Labrador Sea has already penetrated deeply into the equatorial Atlantic within a well-defined deep western boundary undercurrent between 1000 and 2000 m. They estimated that this water has taken about 23 years to reach the equatorial region. Our determination of $\Delta C_{\text{dis eq}}$ is not affected by these very young waters, since our boundary for switching between the ΔC_t^* and the ΔC^* method is at about 2000 m, at the lower boundary of the waters affected by this deep western boundary undercurrent. Furthermore, most of the stations used in the tropics lie

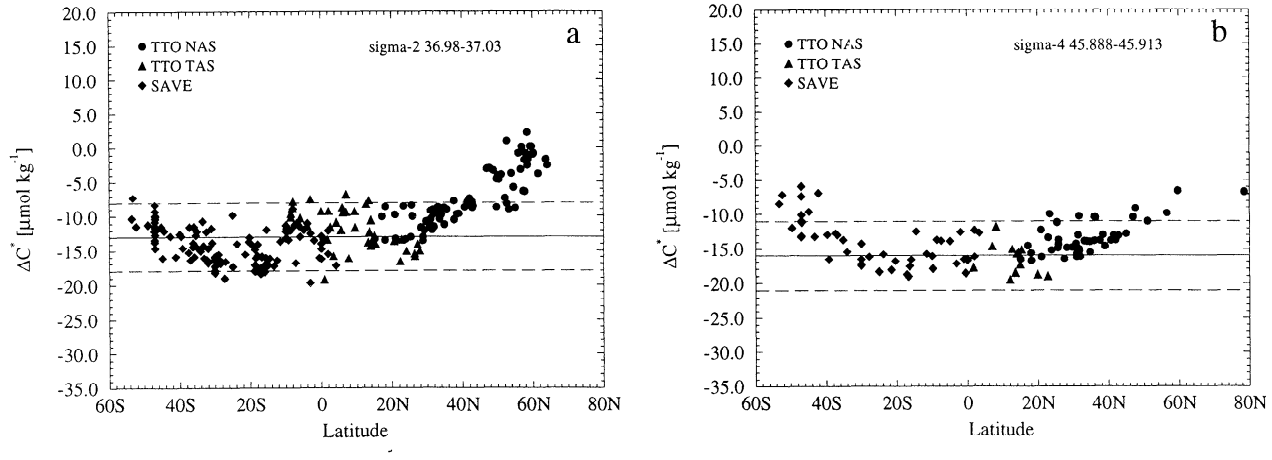

Figure 4. ΔC^* as a function of latitude from 60°S to 80°N along two deep isopycnal horizons in the Atlantic Ocean: (a) the σ_2 interval from 36.98 to 37.03 which represents the core of the North Atlantic Deep Water (NADW) and (b) the σ_4 interval from 45.888 to 45.913 which represents the boundary between the NADW and the Antarctic Bottom Water. The solid lines represents the average ΔC^* in the region from 20°S to 20°N which corresponds to $\Delta C_{\text{dis eq}}$. The dashed lines are drawn at ± 5 μmol kg^{-1} from the estimated $\Delta C_{\text{dis eq}}$, which is a little bit more than half of the estimated error of ΔC^*. The upward trend near the outcrops in the south and the north is due to the invasion of anthropogenic CO_2. Results from the TTO NAS cruises are shown as circles; Results from the TTO TAS cruises as are shown as triangles; and results from the SAVE program are shown as diamonds.

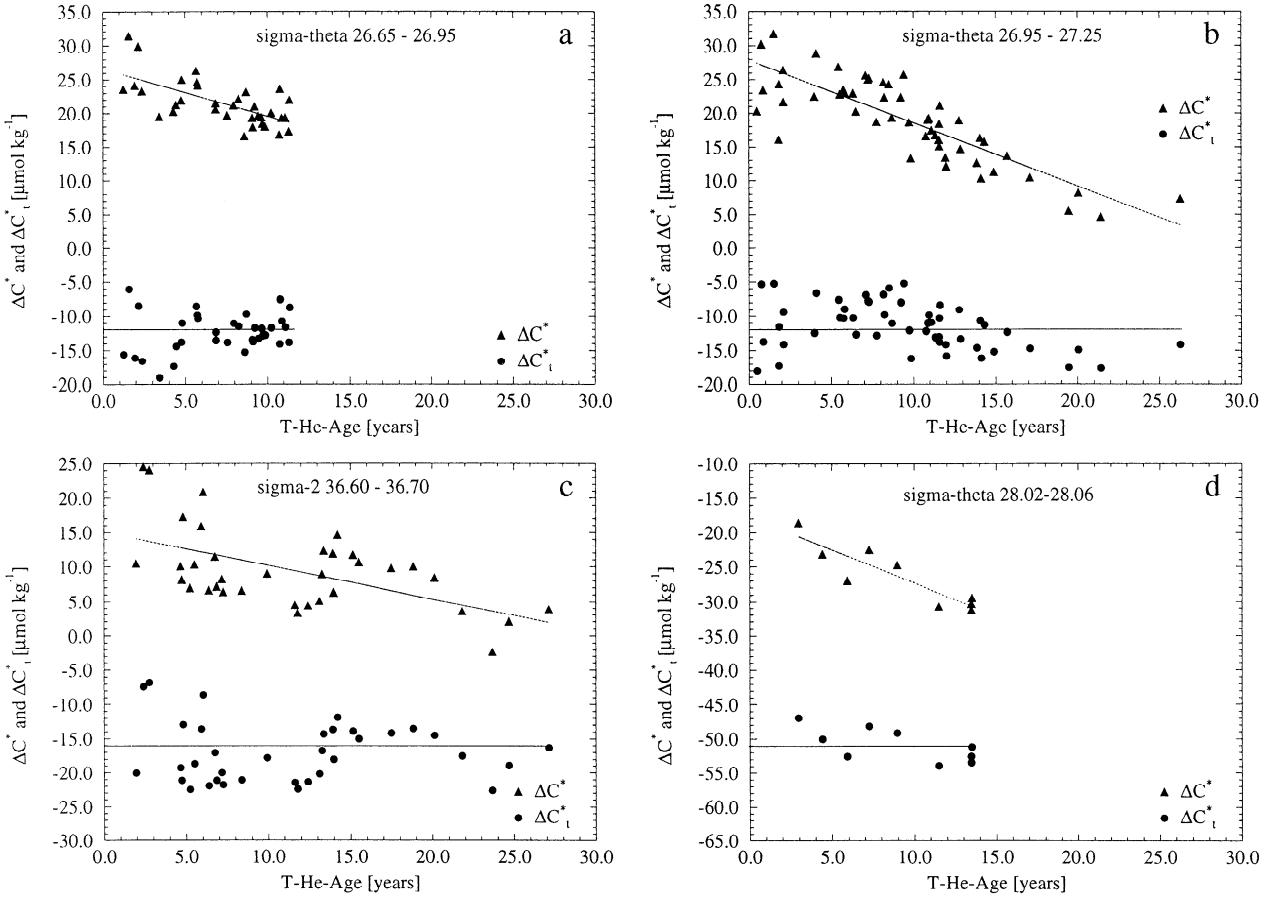

Figure 5. ΔC_t^* (circles) and ΔC^* (triangles) versus tritium-helium age along four isopycnal surface intervals in the North Atlantic. These surfaces include (a) the σ_θ interval 26.65-26.95, (b) the σ_θ interval 26.95-27.25 representing Subpolar Mode Water, (c) the σ_2 interval 36.60-36.70 which lies within the Mediterranean Water Tongue, and (d) the σ_θ interval 28.02-28.06 which occurs only in the Greenland and Norwegian Seas. The lines for ΔC^* are drawn to emphasize the trend and have been obtained by linear regression. The lines for ΔC_t^* represent the average.

well outside the region affected by this western boundary undercurrent.

Figure 5 shows ΔC_t^* and ΔC^* versus ^{3}H-^{3}He age for 4 of the 18 density surfaces where the ΔC_t^* method has been used to estimate the CO_2 air-sea disequilibrium at the time the water lost contact with the atmosphere. These surfaces are the σ_θ interval 26.65-26.95 (average depth 500 m), the σ_θ interval 26.95-27.25 (average depth 700 m) which represents the Subpolar Mode Water [*McCartney and Talley*, 1982], and the σ_2 interval 36.60-36.70 (average depth 1200 m) lying within the Mediterranean Water, and the σ_θ interval 28.02–28.06, which occurs only in the Greenland and Norwegian Seas.

In all surfaces, ΔC^* decreases with increasing water age. This decrease reflects the uptake history of anthropogenic CO_2, since atmospheric fCO_2 was lower when the older water was last in contact with the atmosphere. After removing this effect from ΔC^* by replacing C_{eq} with $C_{eq}(t)$, the resulting ΔC_t^* has more or less constant values within the uncertainties of the scatter of the data. This near constancy of ΔC_t^* also confirms our a priori assumption that the effective air-sea disequilibrium in the outcrop region of a specific density surface has remained constant over time. We determined the final effective CO_2 air-sea disequilibrium, $\Delta C_{\text{dis eq}}$, finally by averaging all ΔC_t^* values within the specified density surface interval using only values with water ages younger than 30 years.

Air-Sea Disequilibrium

A summary of the effective air-sea disequilibrium $\Delta C_{\text{dis eq}}$ found on the isopycnal intervals is given in Table 3 and shown graphically in Figure 6. Also shown are the smoothing spline curves, which are used for the final estimate of ΔC_{ant}. All investigated density surfaces have negative $\Delta C_{\text{dis eq}}$, which means that the outcrop region of these surfaces is undersaturated with respect to atmospheric CO_2. This is due to the fact that all these surfaces outcrop in temperate- to high-latitude

Table 3. Mean Values of Temperature, Salinity, Preformed *Alk*, ΔC_t^*, and calculated ΔfCO_2 on Potential Density Surfaces in the North Atlantic

Potential Density	$\overline{T}$, °C	$\overline{S}$, psu	$\overline{Alk^0}$, μeq kg^{-1}	$\Delta C_{\text{dis eq}}$, μmol kg^{-1}	$\sigma_{\Delta C_{\text{dis eq}}}$, μmol kg^{-1}	$N_{\Delta C_{\text{dis eq}}}$, #	method [a]	ΔfCO_2,[b] μatm
				σ_θ Surfaces				
25.30	23.7	37.06	2417	-19	5	5	2	-26
25.60	22.5	37.04	2417	-17	5	2	2	-24
25.90	20.8	36.82	2405	-13	8	6	2	-19
26.20	18.9	36.60	2393	-24	4	7	2	-35
26.50	17.3	36.42	2385	-22	5	52	2	-32
26.80	14.6	35.97	2364	-12	3	34	2	-20
27.10	11.3	35.50	2343	-12	3	53	2	-20
27.30	9.3	35.29	2333	-14	4	20	2	-25
27.40	8.8	35.31	2335	-17	4	13	2	-30
				σ_2 Surfaces				
36.45	8.1	35.26	2341	-16	5	39	2	-29
36.55	7.4	35.25	2337	-15	5	34	2	-28
36.65	6.4	35.21	2334	-16	6	39	2	-29
36.75	5.5	35.13	2329	-18	5	60	2	-34
36.85	4.4	35.04	2325	-13	8	102	2	-26
36.95	3.8	35.00	2323	-10	4	106	1	-20
37.00	3.1	34.96	2322	-13	4	92	1	-27
37.05	2.7	34.93	2321	-16	3	94	1	-31
				σ_4 Surfaces				
45.825	2.7	34.93	2321	-16	3	51	1	-32
45.850	2.5	34.92	2320	-16	4	49	1	-33
45.875	2.4	34.90	2320	-15	4	68	1	-31
45.900	2.2	34.89	2319	-16	3	39	1	-32
45.925	2.0	34.87	2318	-15	3	28	1	-31
45.950	1.8	34.89	2317	-15	3	15	1	-31
				σ_θ Surfaces in the Greenland and Norwegian Seas				
27.92	2.1	34.91	2319	-36	5	8	2	-67
27.96	1.3	34.91	2318	-43	6	6	2	-80
28.00	0.4	34.90	2318	-41	5	6	2	-77
28.04	-0.4	34.90	2318	-51	3	9	2	-94
28.08	-0.9	34.91	2319	-56	2	34	2	-102

[a] ΔC^* method indicated as 1; ΔC_t^* method indicated as 2.

[b] Calculated from $\overline{T}$, $\overline{S}$, $\overline{Alk^0}$, and $\Delta C_{\text{dis eq}}$ using thermodynamic relationships.

areas characterized by wintertime cooling. The air-sea disequilibrium does not vary greatly in the entire water column of the North Atlantic Ocean south of 60°N. The minimum is about –10 μmol kg^{-1}, and the maximum is about –25 μmol kg^{-1}.

In the main thermocline we find the largest $\Delta C_{\text{dis eq}}$ for the σ_θ surfaces from 26.05-26.60. These surfaces outcrop in the region of Ekman convergence in the North Atlantic between 30°N and 40°N [*Kawase and Sarmiento*, 1985]. The deeper surfaces in the main thermocline (σ_θ 26.65-27.35) show a considerably smaller air-sea disequilibrium. These surfaces also outcrop in the region of Ekman convergence in the North Atlantic but at higher latitudes (40°N - 50°N) [*Kawase and Sarmiento*, 1985]. The waters at the lower base of the thermocline (σ_2 36.40-36.80) have a very uniform $\Delta C_{\text{dis eq}}$ of about –15 μmol kg^{-1}. The source regions of these water masses are the Mediterranean, the Arctic Front and also partially the Antarctic Circumpolar Front (for the Antarctic Intermediate Water). The upper North Atlantic Deep Water (NADW) which is mainly composed of Labrador Sea Water (σ_2

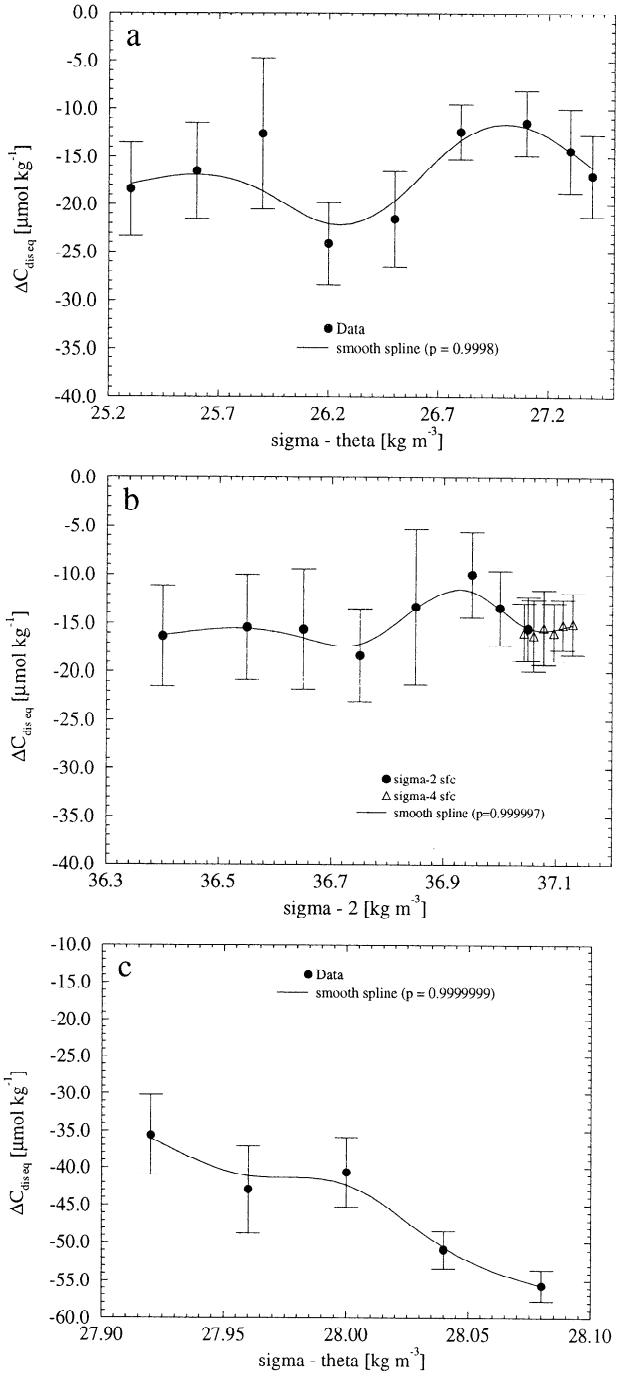

Figure 6. Plot of the estimated $\Delta C_{\text{dis eq}}$ versus potential density for the different potential density intervals. (a) The σ_θ surfaces 25.30-27.40 are shown; (b) the σ_2 surfaces from 36.45-37.05 and the σ_4 surfaces 45.825-45.950 (converted to the appropriate σ_2 value) are shown; and (c) the σ_θ surfaces 27.92-28.08 in the Greenland and Norwegian Seas are shown. Also depicted is a smoothing spline fit through the data. The chosen stiffness parameter p is also shown.

36.80-36.90) has a somewhat lower $\Delta C_{\text{dis eq}}$ than the main body of the NADW (density surfaces σ_2 36.85 to σ_4 45.900) which has a remarkably uniform $\Delta C_{\text{dis eq}}$ of about −15 µmol kg^{-1}. The middle NADW has its source region mainly in the Greenland and Norwegian Seas [*Swift*, 1984a]. We find for the deep waters in these basins a very large $\Delta C_{\text{dis eq}}$ in the range of −36 to −56 µmol kg^{-1}, which is probably due to rapid cooling of surface waters and subsequent deep convection without enough time for CO_2 equilibration. However, the waters overflowing the sills in the Denmark Strait (Denmark Strait Overflow Waters), on Iceland-Faroer Ridge and on Faroer Bank Channel (Iceland Scotland Overflow Waters), which form the source waters for NADW, are not the product of deep convection but of intermediate water formation north of the Greenland-Scotland ridge [*Dickson and Brown*, 1994]. Although not investigated in more detail, one can conclude from the near uniform and relatively low air-sea disequilibrium found in the middle NADW that these intermediate waters in the Greenland and Norwegian Seas must have a much smaller $\Delta C_{\text{dis eq}}$ than the deep waters in these basins.

Is this pattern of CO_2 air-sea disequilibrium consistent with what we know from direct observations of ΔfCO_2? We calculated ΔfCO_2 from $\Delta C_{\text{dis eq}}$ and the mean values of temperature, salinity, and preformed *Alk* along the investigated density surfaces (see Table 3). The same thermodynamic relationships as used in appendix A were employed. In order to calculate zonal means of ΔfCO_2, the outcrop latitudes of all surfaces were first determined from the NOAA Atlas [*Levitus et al.*, 1994; *Levitus and Boyer*, 1994]. Then all calculated ΔfCO_2, which belong to a density surface outcropping within the specified latitude belt, were averaged. We compare our estimate of the zonal mean ΔfCO_2 with the direct wintertime observations of ΔfCO_2 (months December-February) by *Takahashi et al.* [1995, Table 1]. Figure 7 shows very good agree-

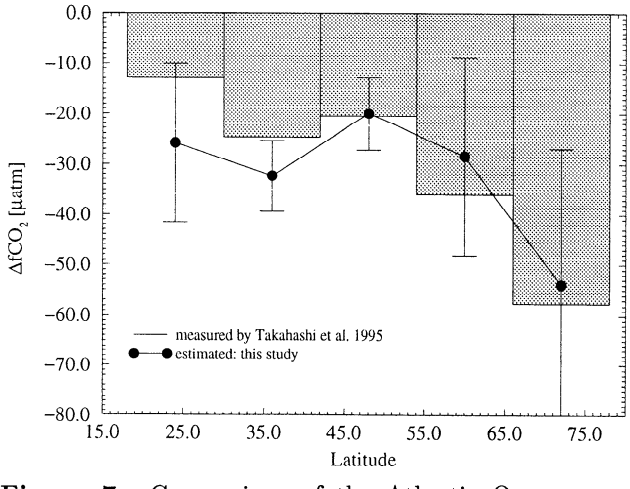

Figure 7. Comparison of the Atlantic Ocean zonal mean air-sea difference of fCO_2, ΔfCO_2, between the observational estimates of *Takahashi et al.* [1995] and our estimates based on $\Delta C_{\text{dis eq}}$. The direct observations are averages for the winter months December-February.

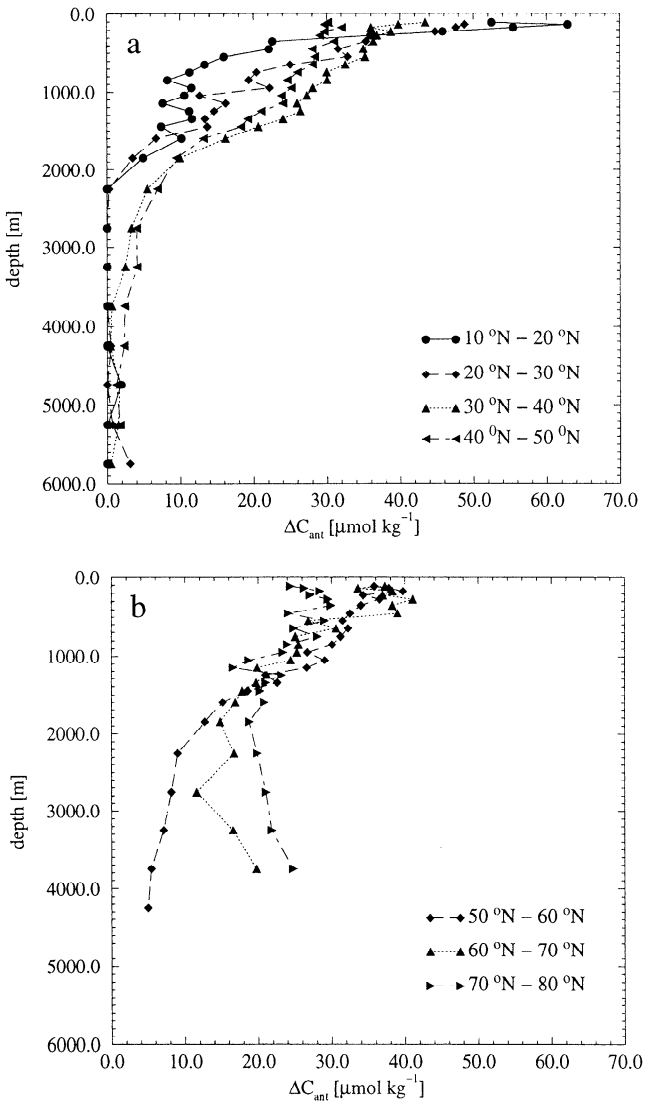

Figure 8. Horizontally averaged profiles of ΔC_{ant} in seven latitude belts from 10°N to 80°N in the North Atlantic.

ment between our estimated ΔfCO_2, based on data from the interior of the ocean and the direct observations. The observations confirm also the relative minimum in the latitude band from 42°N to 54°N and the strong increase of ΔfCO_2 north of 60°N. However, we generally overestimate the air-sea disequilibrium in the low latitudes, where we determine $\Delta C_{dis\ eq}$ by the ΔC_t^* method. In the high latitudes, where the second method employing ΔC^* has been used, the opposite seems to be the case. This tendency is, however, not significant, given the large uncertainties of our estimates of ΔfCO_2 and the observations. This independent check of our approach to estimate the air-sea disequilibrium in the North Atlantic improves our confidence, not only in the determination of $\Delta C_{dis\ eq}$ but also in our estimates of ΔC_{ant}.

Distribution of Anthropogenic CO_2 in the North Atlantic

The results of our separation of the anthropogenic CO_2 component from C are shown in Figures 8 to 10.

Figure 8 shows the horizontally averaged profiles in seven latitude belts from 10°N to 80°N within the North Atlantic. Near the surface (note that we excluded the upper 100 m) the concentrations are in the range of 40 to 50 µmol kg^{-1} in the low latitudes and around 30 µmol kg^{-1} in the high latitudes. This is in agreement with what is expected based on thermodynamic considerations. If the ocean follows more or less the anthropogenic atmospheric CO_2 increase, we expect the cold surface waters (< 5°C) to contain about 30 µmol kg^{-1} of anthropogenic CO_2 and the warm waters (> 20°C) to contain more than 40 µmol kg^{-1} because of the temperature sensitivity of the CO_2 solubility and chemistry.

In the latitude belt from 10°N to 20°N, ΔC_{ant} rapidly decreases downward from the surface to about 10 µmol kg^{-1} at 1000 m depth and to below 2 µmol kg^{-1} at about 2000 m. Going northward, the anthropogenic CO_2 penetrates more and more deeply, which is evident from the increase of ΔC_{ant} at 1000 m and the progressively greater depth at which ΔC_{ant} goes below 2 µmol kg^{-1}. The average profile in the subtropics between 30°N and 40°N shows nearly a linear decrease of ΔC_{ant} between the upper ocean and a depth of about 1500 m. At this depth, ΔC_{ant} is still above 25 µmol kg^{-1}. It then decreases rapidly and goes below 2 µmol kg^{-1} at about 3500 m. The profile in the 40°N to 50°N latitude belt has the same structure as the latitudinal belt to the south. The thermocline, however, contains less anthropogenic CO_2, but there are slightly higher concentrations of ΔC_{ant} in the waters below 2000 m. This trend is confirmed in the latitudinal belt from 50°N to 60°N where ΔC_{ant} stays above 5 µmol kg^{-1} at the greatest depths. The structure of the zonal mean profiles of ΔC_{ant} in the North Atlantic south of 60°N are consistent with our expectation based on the current knowledge of thermocline structure and ventilation [*Rooth and Östlund*, 1972; *Sarmiento et al.*, 1982] and the circulation of the lower limb of the thermohaline overturning [*Doney and Jenkins*, 1994; *Fine*, 1995].

In the latitude belts north of 60°N, ΔC_{ant} shows high concentration down to the bottom. These two latitude belts comprise mainly the Greenland and Norwegian Seas, where the deep water has been shown to be fairly young. *Schlosser et al.* [1995] estimated a tritium-helium age of about 17 years for the Greenland Sea and 30 years for the Norwegian Sea, in good agreement with *Smethie et al.* [1988], who estimated residence times between about 10 and 35 years based on chlorofluoromethane measurements.

Figure 9a depicts a meridional section of ΔC_{ant} from

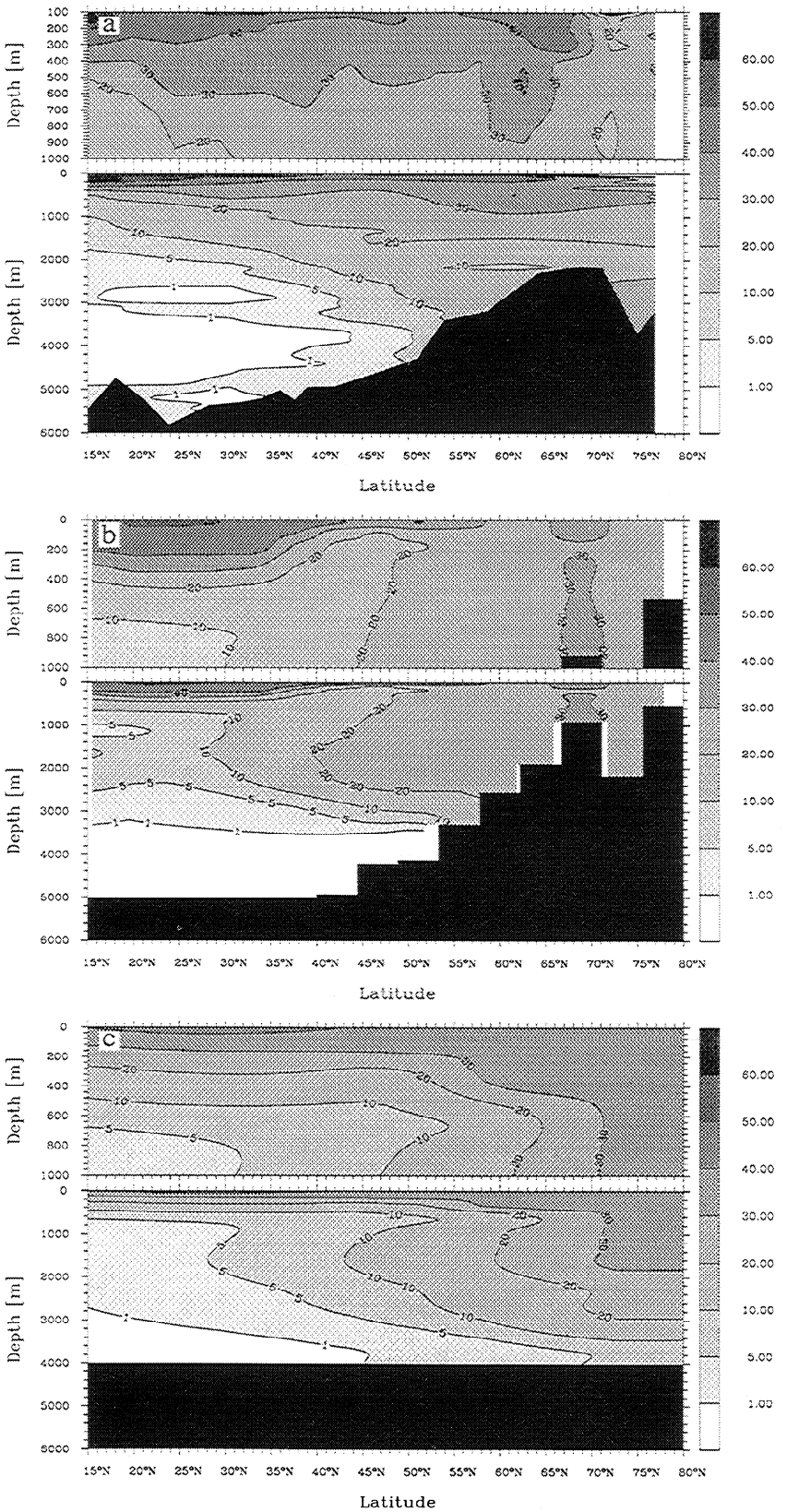

Figure 9. Meridional sections of ΔC_{ant} (μmol kg^{-1}) from 15°N to 80°N in the North Atlantic. (a) observations along the line shown in Figure 2; (b) results from the three-dimensional ocean general circulation biogeochemistry model of *Sarmiento et al.* [1995] along the same line within the resolution of the coarse resolution model; and (c) zonally averaged results from the 2.5-dimensional model of *Stocker et al.* [1994]. The model results are the average values for the year of 1982.

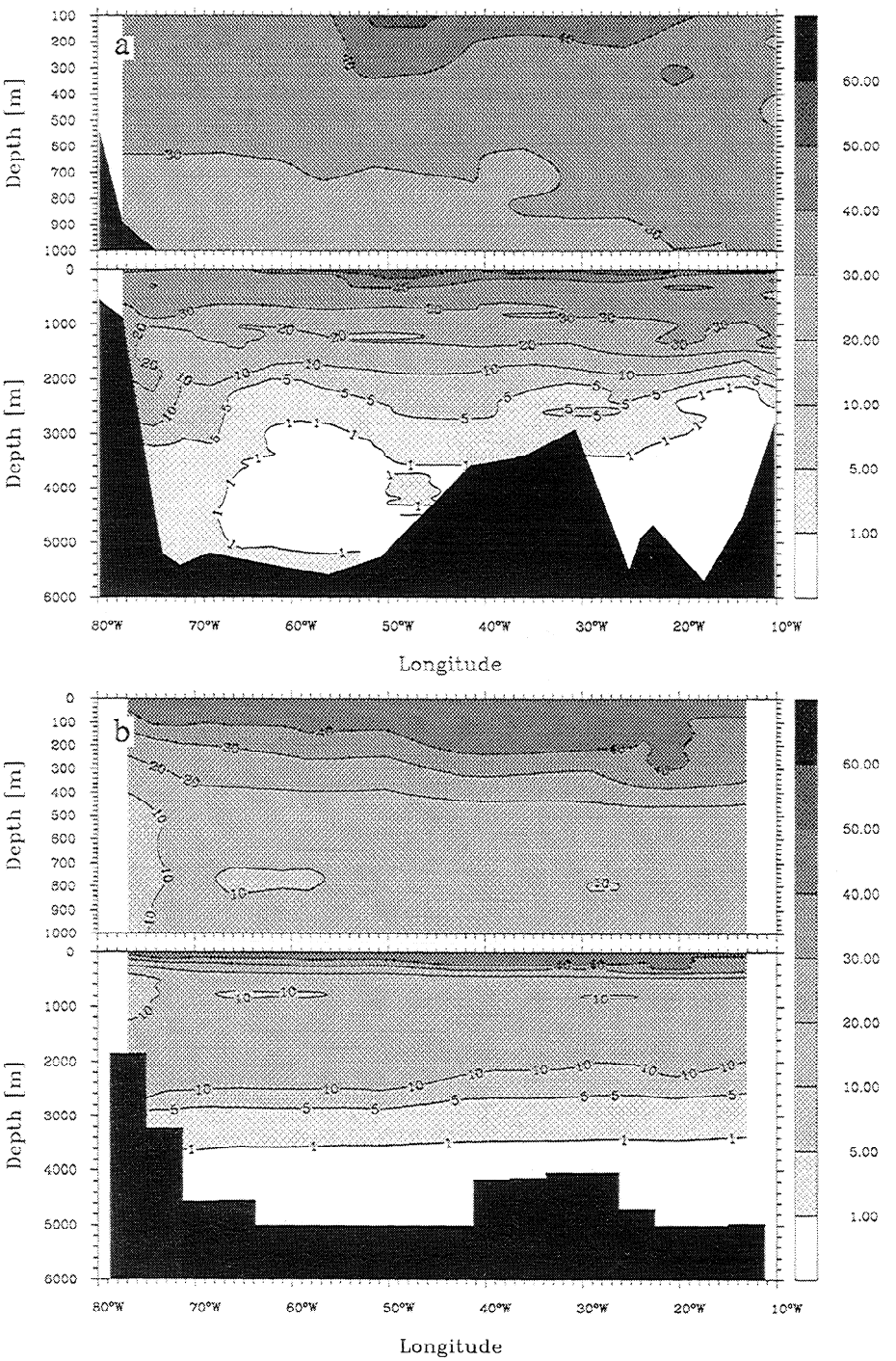

Figure 10. Zonal sections of ΔC_{ant} (μmol kg^{-1}) from 80°W to 10°W in the North Atlantic at approximately 30°N. (a) observations along the line shown in Figure 2 and (b) results from the three-dimensional OGCM biogeochemistry model of *Sarmiento et al.* [1995] for the year of 1982 along the same line within the resolution of the coarse resolution model.

15°N to 80°N in the western Atlantic (see Figure 2 for track). The concentration of anthropogenic CO_2 in the upper 1000 m is rather uniform between 20°N and 60°N. South of 20°N, anthropogenic CO_2 decreases more rapidly with increasing depth than to the north. Below 1000 m, large differences exist between high and low latitudes. The southward spreading of relatively young NADW, which takes with it anthropogenic CO_2, is clearly visible by the downward slope of ΔC_{ant} north of 40°N. Waters below 3000 m and south of 40°N contain essentially no anthropogenic CO_2.

Recent advancement in the understanding of the lower

limb of the thermohaline circulation (see *Fine* [1995] for a review) by the use of transient tracers showed that the deep western boundary undercurrent (DWBC) is transporting freshly formed water in the high latitudes within decades to the tropics [*Doney and Jenkins*, 1994]. Along its pathway it constantly exchanges water with the interior abyssal ocean. We therefore expect to see elevated concentrations of ΔC_{ant} in the western deep Atlantic compared to the eastern basin. Figure 10a shows a zonal section of ΔC_{ant} from 80°W near the North American continent to 10°W close to the Iberian Peninsula at a latitude of approximately 30 °N (see Figure 2 for track). A significant downward slope of the isolines by about 1000 m can be identified near the western boundary below 1000 m. The DWBC at that latitude is split into a shallow core centered at about 1200 m and a deep core centered at about 3500 m [*Fine*, 1995]. Our data do not permit us to discern two separated cores, but the observation of elevated ΔC_{ant} concentration in that region in our section is consistent with our expectation.

This meridional section also reveals a deeper penetration of ΔC_{ant} in the eastern thermocline compared to the west. This pattern reflects primarily the anticyclonic gyre transport, where anthropogenic CO_2, much like bomb tritium, is subducted into the thermocline in the northeast [*Sarmiento et al.*, 1982].

Anthropogenic CO_2 Inventories

On the basis of TTO NAS and TTO TAS data we now estimate the ocean inventory of anthropogenic CO_2 at the time of these surveys (1981-1983). We determine the inventory of each latitudinal belt between latitude φ_1 and φ_2, $\mathrm{INV}(\varphi_1, \varphi_2)$, by vertically integrating the area-weighted mean of ΔC_{ant} in that latitude belt, $\overline{\Delta C_{ant}}(\varphi, z)$,

$$\mathrm{INV}(\varphi_1, \varphi_2) = \int_{\mathrm{bottom}}^{\mathrm{sfc}} A(\varphi, z)\overline{\Delta C_{ant}}(\varphi, z)\, dz, \tag{25}$$

where $A(\varphi, z)$ is the horizontal area of the latitude belt φ between φ_1 and φ_2 as a function of depth as determined from a 1° global topography [*Gates and Nelson*, 1975]. The concentration of ΔC_{ant} in the surface 100 m is estimated from the averaged concentration between 100 and 200 m. We also calculate the specific inventories in the latitude belts ($\mathrm{INV}_{\mathrm{spec}}(\varphi_1, \varphi_2)$) by

$$\mathrm{INV}_{\mathrm{spec}}(\varphi_1, \varphi_2) = \frac{\mathrm{INV}(\varphi_1, \varphi_2)}{A(\varphi, z = 0\,\mathrm{m})}. \tag{26}$$

The results are shown in Table 4. We obtain for the North Atlantic Ocean between 10°N and 80°N a total inventory of about 16.3 $\cdot 10^{14}$ mol C or about 19.6 Gt C and a specific inventory of about 41 mol C m^{-2}. We estimate the error of the inventory (1-σ of the mean) to be about 3.3 $\cdot 10^{14}$ mol C or 4 Gt C (20%) based on the previously estimated signal to noise ratio of ΔC_{ant}. The inventories of the different latitude belts vary greatly because of the strongly varying volumes of these regions in the North Atlantic. The Atlantic Ocean from 10°N to 40°N contains about 64% of the anthropogenic CO_2 inventory, whereas the region from 40°N to 80°N holds the remaining 36%. The reason for this is that the volume of the region from 10°N to 40°N is about 76% of the total volume in the investigated region in the North Atlantic.

We turn therefore to the specific inventories as a better representation of the regions where anthropogenic CO_2 has accumulated. Although most of the effect of ocean topography has been removed, the distribution of the specific inventories is far from being uniform (see Figure 11). The highest specific inventory is found in the subtropical region between 30°N and 40°N with almost 60 mol C m^{-2}. The tropics and the high latitudes have significantly lower specific inventories. The explanation for this pattern is related to the wind-driven meridional circulation. Anthropogenic CO_2 entering the ocean in the equatorial regions and subpolar gyres,

Table 4. Summary of the Estimated Water Column Inventory of Anthropogenic CO_2 in the North Atlantic Ocean by Latitude Belt

Latitude Belt, deg	Surface Area, 10^{12} m^2	Volume, 10^{16} m^3	Number of stations	Specific Inventory, mol C m^{-2}	Inventory, 10^{14} mol C	Inventory, Gt C
10°N - 20°N	8.0	3.1	41	34	2.7	3.3
20°N - 30°N	8.9	3.6	53	41	3.6	4.3
30°N - 40°N	7.0	2.9	85	59	4.2	5.0
40°N - 50°N	5.3	1.6	26	43	2.3	2.8
50°N - 60°N	4.8	0.9	60	40	1.9	2.3
60°N - 70°N	3.7	0.4	22	28	1.0	1.2
70°N - 80°N	2.3	0.2	14	25	0.6	0.7
Total	40.0	12.6	301	41 (mean)	16.3	19.6

which are dominated by upwelling, is laterally transported by Ekman transport to the subtropical gyre where it accumulates in the main thermocline, which is at its deepest at these latitudes [*Sarmiento et al.*, 1992, Figures 5 and 6]. Note also the large accumulation of anthropogenic CO_2 in upper NADW below the main thermocline to a depth of about 3000 m (Figure 9) and in the deep western boundary current (DWBC) (Figure 10). The thermocline shallows and mean ocean depth decreases north of 45°N, both of which gradually reduce the specific inventory. The shallowness of the ocean is the major factor north of 60°N, where the specific inventory is small despite the high deep ocean concentrations.

Comparison With Model Estimates

We compare our estimates of anthropogenic CO_2 in the North Atlantic Ocean with the results of the 2.5-dimensional circulation model of *Stocker et al.* [1994] (SBW) and with the Princeton three-dimensional ocean general circulation biogeochemistry model of *Sarmiento et al.* [1995](SML).

The 2.5-dimensional SBW model is a zonally averaged ocean model, where the world ocean is represented by three ocean basins (Atlantic, Pacific, and Indian) which are connected via a Southern Ocean south of 40°S. An inorganic carbon cycle model has been added representing the solubility pump. The "best tuned" (with respect to temperature and salinity) steady state circulation (state A) is used for the simulations. The inorganic carbon model differs slightly from the model described by *Stocker et al.* [1994], since the surface mean alkalinity [*Takahashi et al.*, 1981] has now been taken as the reference alkalinity instead of the ocean mean value.

The three-dimensional SML model is a coarse resolution model based on the nonseasonal circulation model of *Toggweiler et al.* [1989a]. A full natural carbon cycle model is included, namely, the solubility pump, the soft-tissue pump, and the carbonate pump.

The two models differ in their representation of the carbon cycle. However, since anthropogenic CO_2 can essentially be treated as a conservative tracer which is not involved in biological processes, the representation of the soft-tissue pump and carbonate pumps is not a necessary requirement for the prediction of the uptake of anthropogenic CO_2 [*Broecker*, 1991; *Sarmiento et al.*, 1992].

Both models have been spun up to a preindustrial steady state with an atmospheric CO_2 concentration of 280 μatm for the SML model and 278.9 μatm for the SBW model. To simulate the uptake of CO_2 over the industrial era, the model integrations start in 1767, and atmospheric CO_2 is prescribed for both models by the same smoothing spline through atmospheric CO_2 data obtained from direct observations after 1958 [*Keeling and Whorf*, 1994] and ice-core data before 1958 [*Neftel et al.*, 1994]. Model results are analyzed for the year 1982, which is the middle year of the observations (1981-1983).

The results of these uptake experiments are shown in Tables 5 to 7 and Figures 9 to 11 together with the observations. The agreement between the model inventories in the North Atlantic from 10°N to 80°N (18.7 Gt C for SBW and 18.4 Gt C for SML) and the observed inventory of 20 ± 4 Gt C is very good. The SBW model predicts a 7% higher global uptake rate and 7% higher global inventory than the SML model for the year 1982. However, inventories within the Atlantic from 10°N to 80°N differ by only 1% between the two models. They both slightly underestimate the North Atlantic inventory derived from observations by about 5% to 7%, which is within the uncertainty. The anthropogenic CO_2 inventory is mainly determined by ocean transport [*Siegenthaler and Joos*, 1992; *Sarmiento et al.*, 1992]. The SML model is known to have a too sluggish thermocline ventilation [*Sarmiento et al.*, 1992; *Toggweiler et al.*, 1989b]. However, this seems not to have a great impact on the calculated CO_2 inventory in the North Atlantic. The vertical exchange in the SBW model is too strong in the Southern Ocean because of excessive convection and too weak in the midlatitudes probably because of too little ventilation of the wind-driven gyre [*Stocker et al.*, 1994, p. 117-118]. In the high northern latitudes of the Atlantic the vertical exchange in the SBW model seems to be simulated properly. These two effects counterbalance each other in the Atlantic, causing good agreement between modeled and observed inventories. Note that the SBW model state A was not tuned using radiocarbon data but is rather that state that shows closest agreement of the zonal averages of temperature and salinity in each of the three ocean basins.

Does this good agreement of the anthropogenic CO_2 inventories for the entire North Atlantic also hold regionally? We turn to Figure 9 which shows observed and model calculated meridional sections of ΔC_{ant} in the North Atlantic. Both the SML and the SBW model show qualitative agreement, but there are important differences between them and our reconstruction from the observations. Both models contain significantly less anthropogenic CO_2 in the low-latitude thermocline than predicted by the observations. The isolines are too shallow by about 600 m (SML) and about 400 m (SBW), compared to observations. A particularly large deficiency of anthropogenic CO_2 shows up in the SML model between 40°N and 50°N at depths between 200 and 500 m. This low ΔC_{ant} water is due to artificial upwelling of deep water containing little anthropogenic CO_2 on the landward side of the Gulf Stream [*Togg-*

weiler et al., 1989b, p. 8249]. *Veronis* [1975] pointed out that this artificial upwelling might be due to the strictly horizontal orientation of lateral mixing in the models. Isopycnal mixing helps to reduce this artificial upwelling and also enhances ΔC_{ant} penetration in the thermocline [*Danabasoglu et al.*, 1994]. The 2.5-dimensional SBW model does not show such a depression of ΔC_{ant} in the thermocline of the temperate latitudes, but the deficiency of ΔC_{ant} in the entire thermocline is even larger than in the SML model. The thermocline ventilation process in the 2.5-dimensional model is parameterized by an increased horizontal diffusion. Our result here may indicate that an even higher horizontal diffusion is necessary to account for the high anthropogenic CO_2 present in the thermocline of the temperate latitudes.

Both models simulate the downward depression of the isolines in the high latitudes due to the southward progression of anthropogenic CO_2 bearing NADW. In the SML model the maximum penetration of the NADW does not go below model layer 10 (2935 m) [*Toggweiler et al.*, 1989a], since denser water of Antarctic origin spreads to the north in levels 11 and 12, filling up the entire deep North Atlantic. This water is very weakly ventilated by flow from the south and by vertical mixing and hence contains no anthropogenic CO_2. The SML model overpredicts the concentration of ΔC_{ant} in the NADW (see 10 and 20 μmol kg^{-1} isolines), compensating for the underprediction in the thermocline.

Differences of ΔC_{ant} in the deep ocean between the 2.5-dimensional SBW model and the observations can mainly be attributed to the simplified basin topography. Strong vertical overturning in the northernmost grid - cell at 72.5°N transports large quantities of anthropogenic CO_2 to the model's bottom at 4000 m depth, whereas in the real ocean and the three-dimensional model this deep penetration is prevented by the topography.

Similar success and deficiency of the SML model can be found in a comparison between a simulated and observed zonal section of ΔC_{ant} in the North Atlantic at about 30°N (see Figure 10). As in the observations, the SML model does not show large zonal gradients in ΔC_{ant} at this latitude. Also, very evident is the too shallow penetration of the 30 μmol kg^{-1} isoline and the too deep 10 μmol kg^{-1} isoline. Contrary to the observations, no sign of elevated concentrations near the western boundary can be discerned, although the SML model has a clearly developed western boundary current. The artificial upwelling at the landward side of the western boundary currents is probably responsible for obscuring such a signal.

The too low concentrations in the upper 1000 m between 30°N and 45°N in the SML model are also evident in a more detailed comparison of the model predicted and the observed specific inventories (Table 5 and Figure 11). The model underpredicts the specific inventory in the subtropics from 27°N to 36°N by more than 35%. The total inventory between 10°N and 80°N, however, agrees well, since the overprediction of the specific inventories by the model in the temperate and subpolar regions compensates for this. Comparison of the specific inventories between observations and the SBW model in Table 6 shows large differences in the different latitude belts, which compensate each other, yielding a very good overall agreement. The model calculated specific inventory is only half as large in the tropical to temperate latitudes but almost 4 times larger in the high latitudes. As has been already stated above, the large overprediction of the high-latitude specific inventory can mainly be attributed to the simplified topogra-

Table 5. Comparison of the Estimated Water Column Inventory of Anthropogenic CO_2 in the North Atlantic With Estimates From the *Sarmiento et al.* [1995] (SML) Three-Dimensional Model for the Year 1982 by Latitude Belt

Latitude Belt,	SML Model			Observations		
	Surface Area, 10^{12} m^2	Inventory, Gt C	Specific Inventory, mol C m^{-2}	Surface Area, 10^{12} m^2	Inventory, Gt C	Specific Inventory mol C m^{-2}
9°N - 18°N	6.8	2.4	30	7.0	3.3	39
18°N - 27°N	8.0	3.0	31	8.0	3.3	35
27°N - 36°N	7.1	3.1	36	7.0	4.7	56
36°N - 45°N	5.4	3.0	46	5.5	3.5	53
45°N - 53°N	4.1	2.5	51	4.0	2.0	42
53°N - 62°N	4.4	2.2	42	4.8	2.0	35
62°N - 71°N	3.1	1.4	38	2.8	0.8	25
71°N - 80°N	3.3	0.8	21	1.8	0.5	23
Total	42.2	18.4	36 (mean)	40.9	20.1	41 (mean)

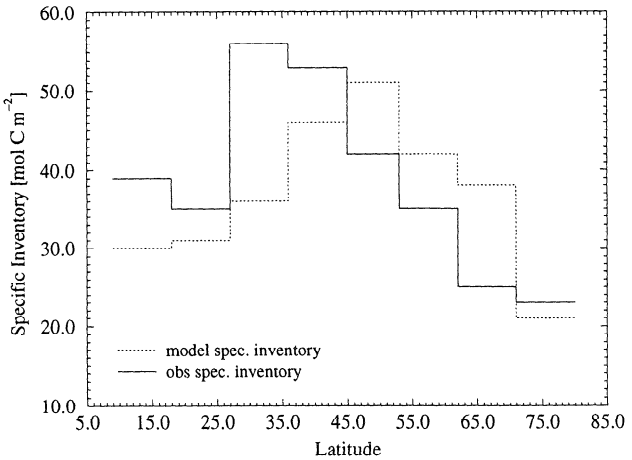

Figure 11. Comparison between observed and OGCM-calculated specific inventories of anthropogenic CO_2 in the North Atlantic. The calculated inventories are from the three-dimensional OGCM biogeochemistry model of *Sarmiento et al.* [1995] and refer to the year of 1982.

phy of the model, whereas the too small specific inventory in the low latitudes is due to a too weak thermocline ventilation. The SBW model has primarily been designed for simulation of the thermohaline circulation and its variability over long timescales, and therefore a detailed comparison of such a 2.5-dimensional model on a regional basis is probably beyond feasibility.

Comparison With Chen's Estimate

Recently, *Chen* [1993] summarized all of his calculations and attempted to estimate a global inventory of the amount of excess CO_2 in the oceans. He found a global inventory of 82.3 ± 16.0 Gt C which is considerably smaller than the two model estimates shown in Table 7. For the North Atlantic ocean from 0° to 65°N he calculated an inventory of 21.5 ± 4.5 Gt C for the year 1972 based on his earlier work [*Chen*, 1982]. He also presented an inventory of 0.85 ± 0.2 Gt C for the Greenland and Norwegian Seas for the year 1982 making use of the study of *Chen et al.* [1990]. Adding these two estimates for the North Atlantic together, disregarding the 10-year difference between them, he finds a total inventory of 22.4 ± 4.5 Gt C between 0°N and 80°N. This is in good agreement with our estimate of 20 ± 4 Gt C for the 10°N to 80°N band, particularly, if one takes into consideration that the 0° to 10°N band has an additional 2-3 Gt C. However, we consider this agreement to be fortuitous because of inherent problems in the Chen approach, as discussed in the introduction, and because of insufficient data coverage. Chen's estimate in the North Atlantic south of Iceland is based on GEOSECS C and Alk data. However, because of problems with the titrators, no reliable carbon data north of 40°N could be obtained during the Atlantic GEOSECS program, and Chen therefore had to extrapolate from data south of 40°N to cover the entire North Atlantic. For his estimate in the Greenland and Norwegian Seas he used wintertime measurements obtained during the Hudson expedition in 1982. However, it was not possible with his technique to find the preindustrial reference level in these basins directly, since anthropogenic CO_2 has penetrated into the whole water column [*Chen et al.*, 1990, p. 1460]. It is therefore unclear to us how *Chen* [1993] was able to estimate an inventory in the Greenland and Norwegian Seas.

Summary and Conclusions

On the basis of three information sources, (1) concurrent measurements of C, Alk, dissolved oxygen, temperature, and salinity on a specific ocean water sample, (2) information about the water age from measurements of tritium and helium isotopes, and (3) the history of the increase of atmospheric CO_2 over the last 200 years, it is possible to separate the anthropogenic CO_2 signal from the large background variability of C in the ocean. This method involves the important assumption of constant $C : O_2$ and $N : O_2$ stoichiometric ratios which is necessary to define a new quasi-conservative tracer ΔC^*

Table 6. Comparison of the Estimated Water Column Inventory of Anthropogenic CO_2 in the North Atlantic With Estimates From the *Stocker et al.* [1994] (SBW) 2.5-Dimensional Model for the Year 1982 by Latitude Belt

Latitude Belt, deg	SBW Model			Observations		
	Surface Area, 10^{12} m^2	Inventory, Gt C	Specific Inventory, mol C m^{-2}	Surface Area, 10^{12} m^2	Inventory, Gt C	Specific Inventory mol C m^{-2}
9°N - 36°N	21.4	5.8	23	22.0	11.3	43
36°N - 62°N	14.6	7.6	43	14.3	7.5	44
62°N - 80°N	5.0	5.4	90	4.6	1.3	24
Total	41.0	18.7	38 (mean)	40.9	20.1	41 (mean)

Table 7. Comparison of the Total Estimated Water Column Inventory of Anthropogenic CO_2 in the North Atlantic With Model Estimates (Year 1982)

	Global Uptake Rate, Gt C yr^{-1}	Global Inventory, Gt C	North Atlantic [a] Inventory, Gt C
Observations (this study)			20 ± 4
Stocker et al. [1994]	1.99	113	18.7
Sarmiento et al. [1995]	1.86	106	18.4

[a]Atlantic Ocean between 10°N and 80°N.

from the information of source 1. This tracer reflects only the uptake of anthropogenic CO_2 and the air-sea disequilibrium when the water parcel lost contact with the atmosphere, plus residual effects due to our choice of oxygen and alkalinity end-members, since the effects of the soft-tissue and carbonate pumps have been removed. Assuming that the ocean has been operating in a steady state and that the effective air-sea disequilibrium has not changed over time, the effective air-sea disequilibrium can be estimated directly from the interior for deep potential density surfaces not entirely affected by anthropogenic CO_2. For the shallower potential density surfaces, information from sources 2 and 3 is used to reconstruct the effective air-sea disequilibrium. This permits us then to identify the anthropogenic CO_2 signal.

We applied this method to carbon and other tracer data from the North Atlantic Ocean sampled as part of the TTO NAS and TAS cruises in 1981 to 1983. The anthropogenic CO_2 distribution in the North Atlantic obtained in this way reflects the pathways of ocean uptake and consequent redistribution within the ocean. Highest concentrations of anthropogenic CO_2 are found in the shallow subtropical thermocline. Vertical penetration is small in the subtropical and temperature latitudes but is large in the high latitudes, because of deep convection and downward transport associated with the NADW. We estimate a North Atlantic anthropogenic CO_2 inventory from 10°N to 80°N of 20 ± 4 Gt C.

We use anthropogenic CO_2 as a constraint to test the performance of two ocean models of different complexity (2.5-dimensional and three-dimensional model) to estimate the uptake of anthropogenic CO_2. The agreement of the total inventory in the investigated region in the North Atlantic is excellent (18.7 Gt C and 18.4 Gt C, respectively), but a regional breakdown reveals important differences, mostly related to known deficiencies in the models.

Our method can be modified and extended easily, by using different methods to estimate the CO_2 air-sea disequilibrium at the time a water parcel was last in contact with the atmosphere. First, there is a possibility to use chlorofluorocarbon observations to derive water ages, since the tritium-helium method fails in the southern hemisphere because of the very small tritium input into this region. Second, the rapidly increasing data set of wintertime measurements of ΔfCO_2 can be used to estimate the CO_2 air-sea disequilibrium more directly.

The strength of this new method will increase when data from the ongoing World Ocean Circulation Experiment (WOCE) will become available in the future. First the high quality carbon data will considerably lower the uncertainty associated with ΔC^* and hence the estimate of anthropogenic CO_2, and second, the global coverage (including transient tracers) will eventually make it possible to calculate a global inventory of anthropogenic CO_2. Repeated surveys in certain regions, where good quality data are already available (Atlantic Ocean) would also permit determination of the increase of the anthropogenic CO_2 over time. These are very powerful constraints for any ocean model employed to estimate the uptake of anthropogenic CO_2.

Appendix A: Preformed Concentrations

Preformed Alkalinity

Our estimate of preformed *Alk* assumes that the anthropogenic transient has not affected the surface alkalinity in the oceans. The invasion of anthropogenic CO_2 affects the degree of equilibrium between C and calcite and aragonite, respectively. However, since surface waters are highly supersaturated with respect to these carbonates [*Takahashi et al.*, 1981], the invasion of anthropogenic CO_2 does not lead to any calcite or aragonite dissolution, which would affect alkalinity.

We estimate preformed *Alk* from a multiple linear regression model using the conservative tracers salinity (S) and PO as independent variables. PO is defined as $PO = O_2 - r_{O_2:P}P$ [*Broecker*, 1974]. We chose an O_2 : P ratio of -170 as given by *Anderson and Sarmiento* [1994] rather than Broecker's [1974] original value of -135 or later value of -175 [*Broecker et al.*, 1985b]. Using upper ocean *Alk* data (< 100 m) from the GEOSECS,

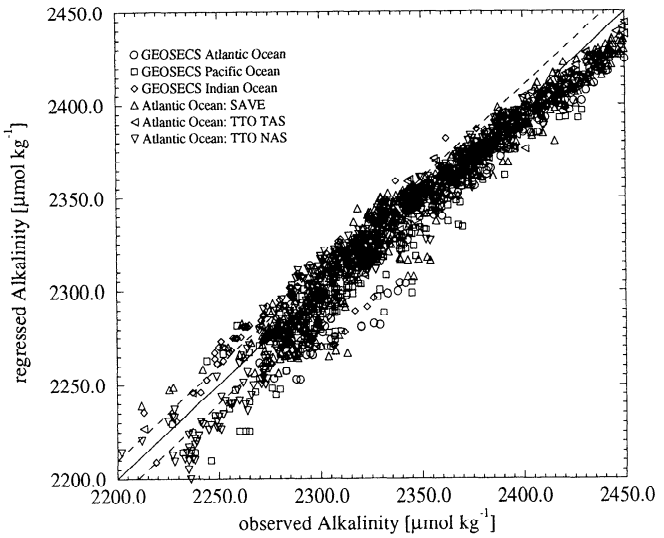

Figure A1. Plot of regressed alkalinity versus observed alkalinity for the world surface oceans. Regressed alkalinity is based on the multiple regression using salinity and the conservative tracer "*PO*" [*Broecker*, 1974] (see (A1)). The dashed curves depict the estimated 1-σ uncertainty of the multiple regression (11 μeq kg^{-1}). The multiple regression underpredicts the alkalinity at very high alkalinity concentrations. However, alkalinities of over 2400 μmol kg^{-1} occur only in the subtropical South Atlantic, and therefore only a small water mass (Subtropical Underwater) is affected.

TTO NAS, TTO TAS, and the SAVE programs gives the following relationship:

$$Alk^0 = (367.5 + 54.9\,\mathrm{psu}^{-1} \cdot S + 0.074\,\mathrm{kg}\,\mu\mathrm{mol}^{-1} \cdot PO)\ \mu\mathrm{eq\ kg}^{-1} \quad : r^2 = 0.96, \tag{A1}$$

where S and PO are in the appropriate units (practical salinity units and micromoles per kilogram, respectively). The standard error of the estimated Alk^0 is 11 μeq kg^{-1} (see Figure A1). This relationship holds for the entire surface ocean as covered by the above cruises. These data have been collected primarily during summer conditions. However, studies at time - series locations in subtropical regions at station "S" and at the Hawaii Ocean Time - Series station (HOT) [*Keeling*, 1993] and high-latitude areas at stations around Iceland [*Takahashi et al.*, 1993] showed that alkalinity, after normalization to constant salinity, reveals little seasonal cycle. The relationship (A1) should therefore yield good results for winter as well as summer conditions.

Takahashi et al. [1980] discussed in detail the alkalinity trends in the surface GEOSECS alkalinity data. For most of the warm waters of the oceans, surface alkalinity is primarily determined by the water balance at the sea surface, yielding very strong correlations with salinity. Waters from the Southern Oceans and the North Pacific show a different trend which is caused by the upwelling of alkalinity rich deep waters produced by dissolution of calcium carbonates [*Takahashi et al.*, 1980, p. 312 ff]. Since these waters also have high PO, inclusion of this tracer as an independent variable greatly improves the predictive value of the regression. Our regression systematically underpredicts the preformed alkalinity at very high alkalinities ($Alk^0 > 2400$ μeq kg^{-1}) (see Figure A1). These high alkalinities occur only in the subtropical South Atlantic Ocean, where alkalinity rich water from the south is undergoing strong evaporation thereby increasing Alk even more. Inclusion of temperature or silicate as independent variables does not help to solve this systematic underprediction. However, the affected water masses occur only in the upper 200 m in the subtropical South Atlantic, and therefore this deficiency does affect our analysis of anthropogenic CO_2 in the North Atlantic.

Chen and Pytkowicz [1979], *Chen and Millero* [1979], and later studies used temperature instead of PO as an independent variable. However, no single relationship was found for the entire ocean surface. This approach represents a large drawback because this introduces serious problems when waters originating from sources with a different relationship are mixed. No such problem exists in our relationship using PO.

Preformed O_2

We assumed in (15) in the main text that dissolved oxygen in the ocean is in equilibrium with the atmosphere when the water parcel loses its contact with the atmosphere, and therefore set O_2^0 equal to O_2^{sat}. Although air-sea exchange of oxygen is rather rapid, the surface waters of the ocean are often supersaturated or undersaturated. *Broecker et al.* [1985a] combined GEOSECS, NORPAX, and TTO surface data and found an average surface supersaturation of 7 μmol kg^{-1}. However, all these measurements were obtained during the summer period. Measurements obtained at time - series stations in subtropical regions (station "S" and HOT) show that the oxygen disequilibrium has a strong seasonality [*Jenkins and Goldman*, 1985; *Emerson et al.*, 1993]. Supersaturation is highest in spring and summer when photosynthesis near the ocean surface is adding oxygen to the surface mixed layer. During the winter months, when most of the deeper waters are formed, O_2 is very close to its saturation value. Time series stations in the subarctic (station "P" and stations around Iceland) show the same seasonal behavior [*Emerson*, 1987; *Takahashi et al.*, 1985b; *Takahashi et al.*, 1993]. Wintertime measurements during the Hudson cruise in the Norwegian and Greenland Seas also showed oxygen concentration near saturation [*Chen et al.*, 1990]. We therefore conclude that the average

supersaturation found by *Broecker et al.* [1985a] is an upper limit because it is summer-biased and that the average deep water formed during the winter season is near saturation for oxygen. However, to account for possible disequilibria, we assign an uncertainty of about 4 μeq kg^{-1} (1-2%) to O_2^{sat} based on the results of the time - series stations and the Hudson cruise.

Calculation of C_{eq}

In order to keep the definition of ΔC^* conservative, we linearize C_{eq} around ocean mean values of temperature, salinity, and alkalinity. The equilibrium concentration of C with respect to an atmospheric CO_2 fugacity of 280 μatm was first calculated using the dissociation constants for carbonic acid of *Goyet and Poisson* [1989], the dissociation constant for boric acid of *Dickson* [1990], the dissociation constant for water in seawater of *Dickson and Riley* [1979a], the dissociation constants for phosphoric acid of *Dickson and Riley* [1979b], and the CO_2 solubility of *Weiss* [1974]. The linearization of C_{eq} yields

$$\begin{aligned} C_{eq}(S,T,Alk)\,|_{fCO_2 = 280\,\mu atm} = \\ [2072.0 - 8.982\,^\circ C^{-1} \cdot (T - 9.0\,^\circ C) \\ - 4.931\,psu^{-1} \cdot (S - 35.0\,psu) \\ + 0.842\,kg\,\mu eq^{-1} \cdot (Alk - 2320.0\,\mu eq\,kg^{-1})] \\ \mu mol\,kg^{-1}, \end{aligned} \tag{A2}$$

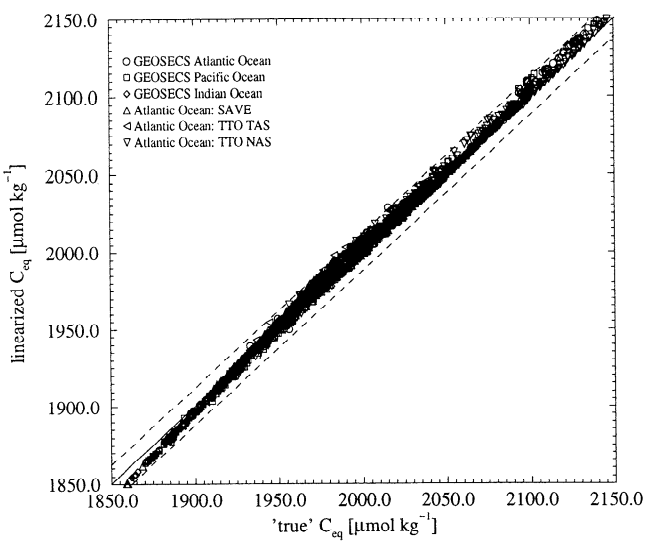

Figure A2. Plot of linearized C equilibrium concentration $C_{eq}(S,T,Alk)$ (see (A2)) versus directly calculated C equilibrium concentration using the full carbon chemistry equations. These equilibrium concentrations are for an atmospheric fCO_2 of 280 μatm. This plot is based on surface (< 100 m) temperature, salinity, and alkalinity data from the GEOSECS, TTO, and SAVE cruises. The dashed curves represent the the estimated 1-σ uncertainty of 4 μmol kg^{-1}.

where T denotes the temperature (degrees Celsius), S denotes the salinity (practical salinity units), and Alk denotes the alkalinity (μeq kg^{-1}). Using the observed temperature, salinity, and alkalinity data of the GEOSECS, TTO and SAVE cruises, the 1-σ standard deviation of the difference between the linearized equilibrium concentration C_{eq} and the directly calculated C_{eq} is found to be about 3 μmol kg^{-1} (see Figure A2). However, for waters with a very low or very high C_{eq}, the discrepancy can be as large as 8 μmol kg^{-1}. To account for this, we increase the uncertainty of the linearized equilibrium concentration C_{eq} to 4 μmol kg^{-1}. When C_{eq} is used in context of (15), Alk is replaced by Alk^0.

Appendix B: Data Considerations

Measurement Methods, Precision, and Accuracy

The C and Alk determinations during the GEOSECS program employed a potentiometric titration technique followed by a Gran type processing of the titration output [*Bradshaw et al.*, 1981]. The precision of the Alk data is estimated to be about ± 9 μeq kg^{-1}, and for C it is about ± 10 μmol kg^{-1} [*Brewer et al.*, 1986]. The Alk data during the TTO NAS and TAS cruises were obtained by a slightly revised potentiometric technique [*Brewer et al.*, 1986] which resulted in an improved precision of about ± 5 μeq kg^{-1}. The C data were also obtained from the titration, but in the case of the TTO NAS cruise these were not used in our study. Instead, the C data were calculated from the Alk and fCO_2 measurements using thermodynamic relationships [*Takahashi and Brewer*, 1986]. The precision of this recalculated C data is probably similar to the precision of the potentiometric C determinations during the TTO TAS cruise and of the order of ± 5 μmol kg^{-1}. During the SAVE cruise, only fCO_2 and C were measured. The C determinations were done coulometrically with a precision of about 2 μmol kg^{-1} (T. Takahashi, personal communication, 1995). The Alk data were calculated from C and fCO_2. We estimate for Alk a precision of about ± 4 μeq kg^{-1}.

Internal Consistency

We have applied the following corrections (in micromoles per kilogram) to the GEOSECS C, Alk, and P data as summarized by *Anderson and Sarmiento* [1994]:

stations 28-34	C –17	[*Bainbridge*, 1981b, p. 2]
Pacific: C and Alk	various	[*Craig et al.*, 1981, p. 2]
stations 201-454	C –15	[*Takahashi*, 1983, p. 5]
various corrections to P		[*Broecker et al.*, 1985b]

The internal consistency of the Atlantic data sets was investigated by determining deep ocean (>3500 m) C

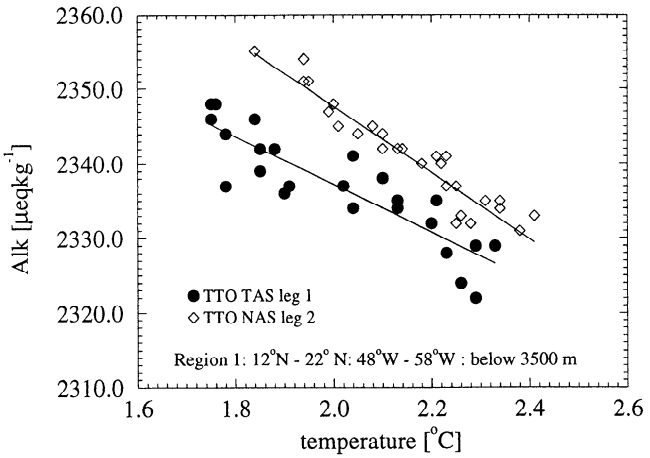

Figure A3. Alkalinity versus temperature in the region from 12°N to 22°N and from 48°W to 58°W and for depths below 3500 m in the North Atlantic. Values for TTO TAS leg 1 are shown by circles and for TTO NAS leg 2 by diamonds. The lines represent the results of linear regressions. A mean difference of 9 μeq kg^{-1} has been found between the two cruises.

and *Alk* trends versus temperature in 10° by 10° areas which have been repeatedly sampled by different legs or cruises. We identified four regions for the TTO NAS, two regions for the TTO TAS, and seven regions for the SAVE program. The revised carbon data from the TTO NAS cruise showed good internal consistency. However, systematic offsets for TTO TAS and SAVE data have been identified.

Comparison of the trends of *Alk* versus temperature in the region from 12°N to 22°N and from 48°W to 58°W and below 3500 m show that the TTO TAS leg 1 measurements are systematically lower by about 9 μeq kg^{-1} than the TTO NAS determinations (see Figure A3). This is almost twice the estimated precision of the *Alk* measurements. Comparison of C, salinity, and nutrient data show no such offset. We therefore conclude that this offset is due to analytical problems and should be corrected for.

A similar offset was identified for the C data of TTO TAS leg 2. In Figure A4, C data from the region from 25°N to 35°N and from 25°W to 35°W and below 3500 m are plotted versus temperature. We calculated a significant mean offset of 13 μmol kg^{-1} between the TTO TAS leg 2 and the TTO NAS C data, with the TTO TAS being higher. No such difference is found in the other tracers analyzed, and we are therefore forced to conclude that this offset is probably not "real".

Comparison of C versus temperature in the region from 10°S to the equator and from 20°W to 30°W and

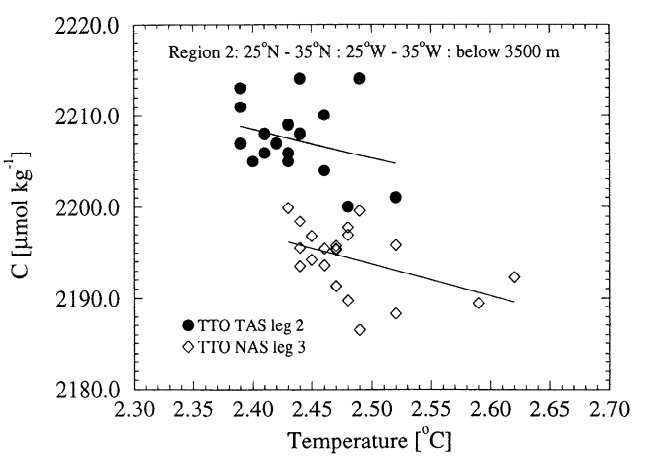

Figure A4. C versus temperature in the region from 25°N to 35°N and from 25°W to 35°W and for depths below 3500 m in the North Atlantic. Values for TTO TAS leg 2 are depicted by circles and for TTO NAS leg 3 by diamonds. The lines represent the results of linear regressions. The mean difference between the two cruises amounts to 13 μmol kg^{-1}.

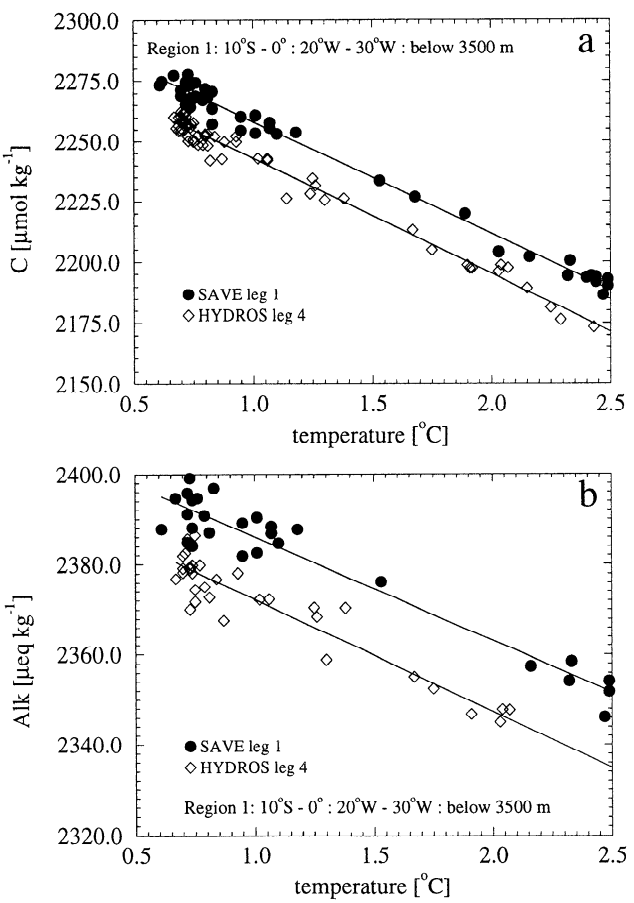

Figure A5. (a) C versus temperature in the region from 10°S to 0° and from 20°W to 30°W and for depths below 3500 m in the Equatorial Atlantic. Values for SAVE leg 1 are shown by circles and for HYDROS leg 4 (equals SAVE leg 6) by diamonds. The lines represent the results of linear regressions. A mean difference of 15 μmol kg^{-1} is found between the two legs. (b) The same for *Alk*. The difference for *Alk* is 19 μeq kg^{-1}.

below 3500 m shows a significant systematic difference between SAVE leg 1 and HYDROS leg 4 (equals SAVE leg 6) of approximately 15 μmol kg^{-1} (Figure A5a). Since the SAVE *Alk* has been calculated from *C* and fCO_2 determinations, this offset should also be evident in the *Alk* versus temperature trend from the same region. As shown in Figure A5b, *Alk* data from SAVE leg 1 is indeed systematically higher by about 19 μeq kg^{-1}, confirming our expectation. We found a similar problem with the *C* and *Alk* data of SAVE leg 2. Figure A6a shows *C* versus temperature in the region from 22°S to 12°S and from 20°W to 30°W and for depths below 3500 m. *C* data from SAVE leg 2 are consistently higher than data from HYDROS leg 4 (SAVE leg 6) by approximately 13 μmol kg^{-1}. The *Alk* data of SAVE leg 2 from the same region also show a systematic offset of about 12 μeq kg^{-1}, as expected (Figure A6b). A comparison of HYDROS leg 4 with the other SAVE legs (except leg 1 and 2) and the corrected TTO TAS data reveals no additional inconsistencies in the *C* and *Alk* data. Investigation of the trends of the other tracers (salinity and nutrients) do not show consistency problems, so that temporal variability can be excluded as a cause. We conclude therefore that the *C* determinations of SAVE leg 1 and 2 have a consistent offset, which then also affected the calculated *Alk* data.

In summary, we found and applied the following corrections to the carbon data:

TTO TAS leg 1 (1-54)	$Alk_{corr} = Alk + 9$ μeq kg^{-1}
TTO TAS leg 2 (55-94)	$C_{corr} = C - 13$ μmol kg^{-1}
SAVE leg 1 (1-43)	$C_{corr} = C - 15$ μmol kg^{-1}
SAVE leg 1 (1-43)	$Alk_{corr} = Alk - 19$ μeq kg^{-1}
SAVE leg 2 (44-105)	$C_{corr} = C - 13$ μmol kg^{-1}
SAVE leg 2 (44-105)	$Alk_{corr} = Alk - 12$ μeq kg^{-1}

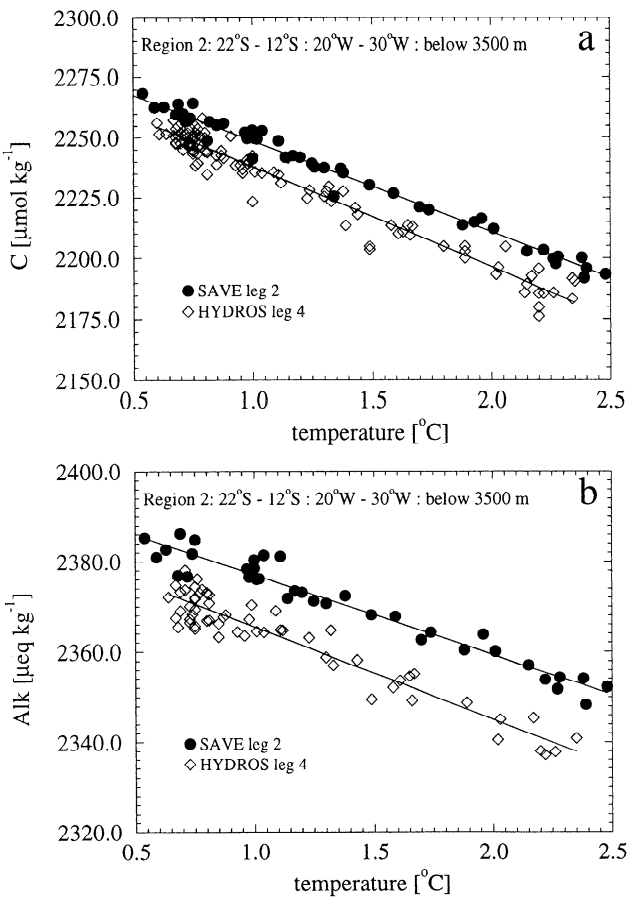

Figure A6. (a) *C* versus temperature in the region from 22°S to 12°S and from 20°W to 30°W and for depths below 3500 m in the Equatorial Atlantic. Values for SAVE leg 2 are shown by circles and for HYDROS leg 4 (equals SAVE leg 6) by diamonds. The lines represent the results of linear regressions. A mean difference of 13 μmol kg^{-1} is found between the two legs. (b) The same for *Alk*. The difference for *Alk* is 12 μeq kg^{-1}.

Accuracy Assessment

We assessed possible inaccuracies of the corrected Atlantic data by comparing them with the shore-based *C* and *Alk* measurements obtained by the Carbon Dioxide Research Group (CDRG) at the Scripps Institution of Oceanography (C.D. Keeling, personal communication, 1994). The CDRG *C* data were measured employing a cryogenic vacuum extraction method with a reported precision of about ±0.5 μmol kg^{-1} and accuracy of about ±1 μmol kg^{-1} (T.J. Lueker et al., Inorganic carbon variations in surface waters near Bermuda, submitted to the *Journal of Marine Chemistry*, 1996)(Hereinafter referred to as Lueker et al., submitted manuscript, 1996). *Alk* was determined using a potentiometric titration with an estimated precision of ±2 μeq kg^{-1} and accuracy of about ±5 μeq kg^{-1} (Lueker et al., submitted manuscript, 1996)

For TTO NAS and TTO TAS, *C* data from CDRG and from *Brewer et al.* [1986] were available from the same bottles. In the case of SAVE, *C* and *Alk* from CDRG and from Oceanographic Data Facility [*ODF*, 1992a; *ODF*, 1992b, T. Takahashi, personal communication, 1995] were available for the same bottles. The revised TTO NAS *C* data no longer have the depth dependency that was described by *Bradshaw and Brewer* [1988], but there is still a substantial amount of scatter in the difference between the *Brewer et al.* [1986] TTO NAS revised *C* data and the CDRG data (see Figure A7a). The mean difference is –3.4 ± 5.1 μmol kg^{-1} (number of samples (N) = 126). The difference between the PCODF [1986b] TTO TAS and the CDRG *C* data is approximately the same (Figure A7b). The mean difference for all depths is –3.6 μmol kg^{-1} with a standard deviation of 5.7 μmol kg^{-1} (N = 77). However, all differences below 200 m are negative, and the mean difference for the data below 1500 m is –5.3 ± 3.7

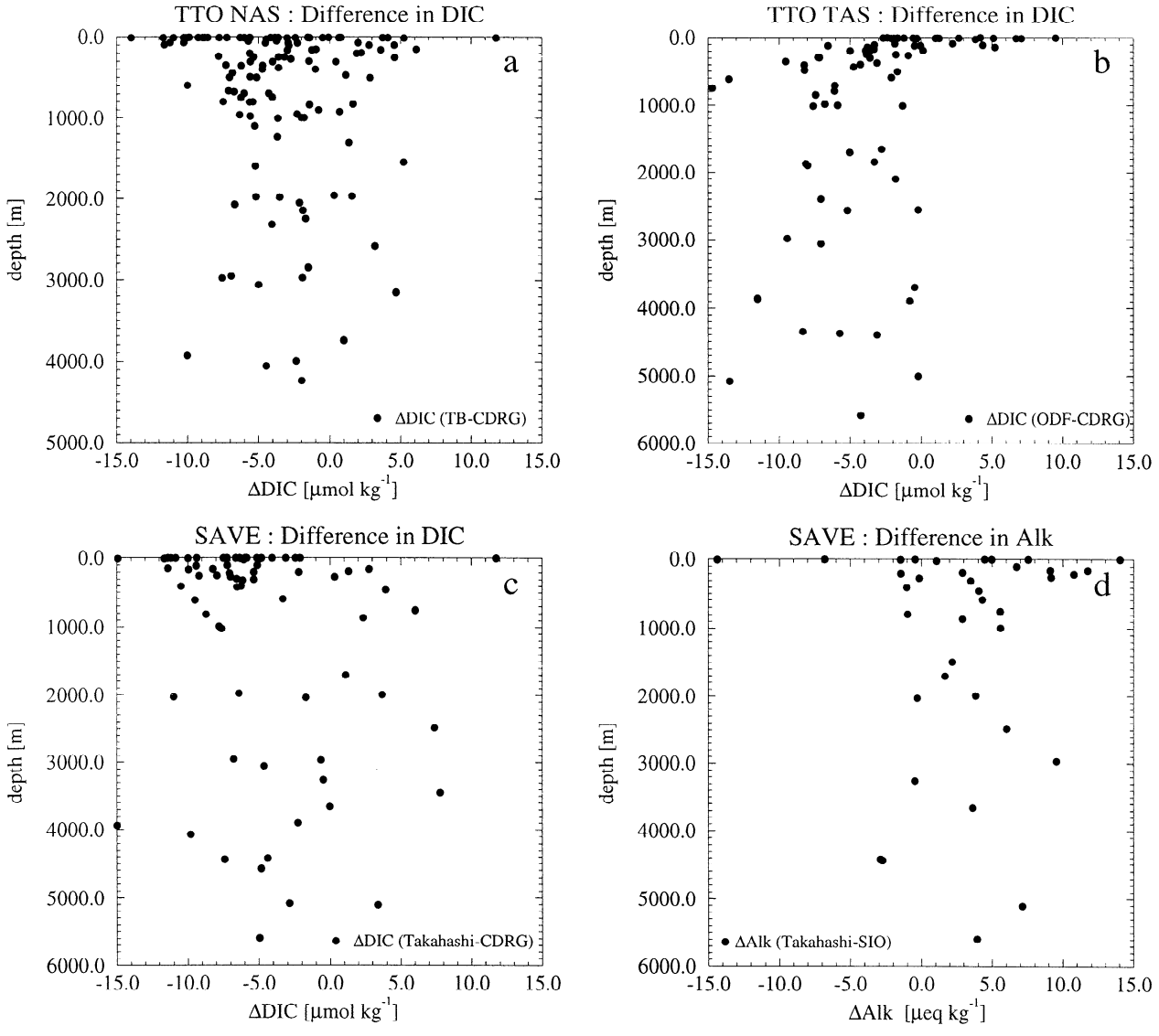

Figure A7. (a) Difference between the *Takahashi and Brewer* [1986] revised TTO NAS and the Carbon Dioxide Research Group (CDRG) TTO NAS C data sets. (b) Difference between the *PCODF* [1986b] TTO TAS and CDRG TTO TAS C data sets. (c) Difference between the corrected T. Takahashi (personal communication, 1995) SAVE and CDRG SAVE C data sets. (d) Difference between the corrected T. Takahashi (personal communication, 1995) SAVE and CDRG SAVE *Alk* data sets. All samples were drawn from the same bottles.

μmol kg^{-1} (N = 20). Although this is a significant systematic difference at the 5% confidence level, we applied no correction to the PCODF TTO TAS data, since this difference is close to the measurement accuracy of these data.

Figure A7c shows the difference between the corrected (T. Takahashi, personal communication, 1995) SAVE and the CDRG C data. The upper ocean Takahashi (personal communication, 1995) C data seem to be systematically lower by approximately 8 μmol kg^{-1}, whereas below 1500 m the difference is –2.9 μmol kg^{-1} with a standard deviation of 5.6 μmol kg^{-1} (N = 21). The mean difference for all depths is found to be –5.1 ± 5.4 μmol kg^{-1} (N = 74) which is significant at the 5% level. However, no further correction has been applied to the SAVE data, since this difference is in the range of the accuracy of the C determinations during this cruise. *Alk* in Figure A7d shows a mean difference over all depths of 3.4 ± 5.6 μeq kg^{-1} (N = 38). This comparison shows that no systematic differences exist between the TTO NAS, TTO TAS, and SAVE C and *Alk* data sets. However, the CDRG C data seem to be consistently higher by 2-3 μmol kg^{-1}. The reason for this discrepancy is presently not known.

Acknowledgments. This study would not have been possible without the careful and painstaking work of the scientists and personnel on the ships during the GEOSECS, TTO, and SAVE programs collecting the data that we depend so heavily upon. We thank C.D. Keeling for providing us his unpublished *C* and *Alk* measurements in the Atlantic Ocean and for the financial support of N.G. during his visit to the Scripps Institution of Oceanography. We are indebted to T. Takahashi for sharing his SAVE carbon data and to W.J. Jenkins for giving us access to his tritium and helium isotope data in the North Atlantic. We would like to thank R. Key for providing the GEOSECS and TTO data in electronic form and very useful oceanographic Fortran routines. Thank goes also to Roger Fink for sharing his carbon chemistry routines. The work of the Oak Ridge Carbon Dioxide Information Analysis Center (CDIAC) in providing many important data sets to the research community is greatly appreciated. C. LeQuéré and R. Murnane are due thanks for providing the code and results of the Princeton OGCM biogeochemistry model. We thank F. Joos for valuable discussions during the preparation of this paper. Reviews by R. Keeling and C.-T.A. Chen helped to improve the article. We appreciate the efforts of M. Bender who served as editor for this article. T.F.S. and N.G. were supported by the Swiss National Science Foundation. J.L.S. was granted support by the National Oceanic and Atmospheric Administration's office of Global Programs, by the National Science Foundation (OCE-9402633) and by the U.S. Department of Energy under contract DE-FG02-90ER61052.

References

Anderson, L. A., and J. L. Sarmiento, Redfield ratios of remineralization determined by nutrient data analysis, *Global Biogeochem. Cycles, 8*(1), 65–80, 1994.

Bainbridge, A., *Hydrographic Data, 1972-1973, GEOSECS Atlantic Expedition*, vol. 1, U.S. Gov. Print. Off., Washington, D.C., 1981a.

Bainbridge, A., *Sections and Profiles, 1972-1973, GEOSECS Atlantic Expedition*, vol. 2, U.S. Gov. Print. Off., Washington, D.C., 1981b.

Boulahdid, M., and J. F. Minster, Oxygen consumption and nutrient regeneration ratios along isopycnal horizons in the Pacific Ocean, *Mar. Chem., 26*, 133–153, 1989.

Bradshaw, A. L., and P. G. Brewer, High precision measurements of alkalinity and total carbon dioxide in seawater by potentiometric titration, 1, Presence of unknown protolyte(s), *Mar. Chem., 23*, 69–86, 1988.

Bradshaw, A. L., P. G. Brewer, and D. K. Shafer, Measurements of total carbon dioxide and alkalinity by potentiometric titration in the GEOSECS program, *Earth Planet. Sci. Lett., 55*, 99–115, 1981.

Brewer, P. G., Direct observation of the oceanic CO_2 increase, *Geophys. Res. Lett., 5*(12), 997–1000, 1978.

Brewer, P., G. Wong, M. Bacon, and D. Spencer, An oceanic calcium problem?, *Earth Planet. Sci. Lett., 26*, 81–87, 1975.

Brewer, P., W. Broecker, W. Jenkins, P. Rhines, J. Swift, T. Takahashi, and R. Williams, A climate freshening of the deep Atlantic north of 50°N over the past 20 years, *Science, 222*, 1237–1239, 1983.

Brewer, P., A. Bradshaw, and R. Williams, Measurements of total carbon dioxide and alkalinity in the North Atlantic ocean in 1981, in *The Changing Carbon Cycle, A Global Analysis*, edited by J. Trabalka and D. Reichle, pp. 358–381, Springer-Verlag, New York, 1986.

Broecker, W. S., 'NO', a conservative water-mass tracer, *Earth Planet. Sci. Lett., 23*, 100–107, 1974.

Broecker, W. S., Chemical signatures associated with the freshening of Northern Atlantic waters between 1972 and 1982, North Atlantic Deep Water Formation, *NASA Conf. Publ., 2367*, 13–17, 1985.

Broecker, W. S., Keeping global change honest, *Global Biogeochem. Cycles, 5*(3), 191–192, 1991.

Broecker, W. S., and T.-H. Peng, *Tracers in the Sea*, Eldigio Press, Lamont-Doherty Geological Observatory, Palisades, N.Y., 1982.

Broecker, W. S., D. Spencer, and H. Craig, *Hydrographic Data, 1973-1974, GEOSECS Pacific Expedition*, vol. 3, U.S. Gov. Print. Off., Washington, D.C., 1982.

Broecker, W. S., T. Takahashi, and T.-H. Peng, Reconstruction of past atmospheric CO_2 from the chemistry of the contemporary ocean: An evaluation, *Tech. Rep. TRO 20*, U.S. Dep. of Energy, Washington, D.C., 1985a.

Broecker, W. S., T. Takahashi, and T. Takahashi, Sources and flow patterns of deep-ocean waters as deduced from potential temperature, salinity, and initial phosphate concentration, *J. Geophys. Res., 90*(C4), 6925–6939, 1985b.

Broecker, W. S., S. Blanton, W. M. Smethie, and G. Ostlund, Radiocarbon decay and oxygen utilization in the deep Atlantic Ocean, *Global Biogeochem. Cycles, 5*(1), 87–117, 1991.

Chen, C.-T. A., On the distribution of anthropogenic CO_2 in the Atlantic and Southern Oceans, *Deep Sea Res., 29*(5A), 563–580, 1982.

Chen, C.-T. A., The oceanic anthropogenic CO_2 sink, *Chemosphere, 27*(6), 1041–1064, 1993.

Chen, C.-T. A., and F. J. Millero, Gradual increase of oceanic CO_2, *Nature, 277*, 205–206, 1979.

Chen, C.-T. A., and R. M. Pytkowicz, On the total CO_2-titration alkalinity oxygen system in the Pacific Ocean, *Nature, 281*, 362–365, 1979.

Chen, C.-T. A., E. P. Jones, and K. Lin, Wintertime total carbon dioxide measurements in the Norwegian and Greenland Seas, *Deep Sea Res., 37*(9), 1455–1473, 1990.

Chen, C.-T. A., S.-L. Wang, and A.S.Bychkov, Carbonate chemistry of the Sea of Japan, *J. Geophys. Res., 100*(C7), 13737–13745, 1995.

Craig, H., W. Broecker, and D. Spencer, *Sections and Profiles, 1973-1974, GEOSECS Pacific Expedition*, vol. 4, U.S. Gov. Print. Off., Washington, D.C., 1981.

Danabasoglu, G., J. C. McWilliams, and P. R. Gent, The role of mesoscale tracer transports in the global ocean circulation, *Science, 264*, 1123–1126, 1994.

Dickson, A. G., Thermodynamics of the dissociation of boric acid in synthetic seawater from 273.15 to 318.15 K, *Deep Sea Res., 37*(5), 755–766, 1990.

Dickson, A. G., and J. Riley, The estimation of acid dissociation constants in seawater media from potentiometric titrations with strong base, I, The ionic product of water - Kw, *Mar. Chem., 7*, 89–99, 1979a.

Dickson, A. G., and J. Riley, The estimation of acid dissociation constants in seawater media from potentiometric titrations with strong base, II, The dissociation of phosphoric acid., *Mar. Chem., 7*, 101–109, 1979b.

Dickson, R. R., and J. Brown, The production of North Atlantic Deep Water: Sources, rates, and pathways, *J. Geophys. Res., 99*(C6), 12319–12341, 1994.

Doney, S., and W. Jenkins, Ventilation of the deep western boundary current and abyssal Western North Atlantic: Estimates from tritium and ^{3}He distributions, *J. Phys. Oceanogr., 24*, 638–659, 1994.

Emerson, S., Seasonal oxygen cycles and biological new pro-

duction in surface waters of the subarctic Pacific Ocean, *J. Geophys. Res., 92*(C6), 6535–6544, 1987.

Emerson, S., P. Quay, C. Stump, D. Wilbur, and R. Schudlich, Determining primary production from the mesoscale oxygen field, *ICES Mar. Sci. Symp., 197*, 196–206, 1993.

Enting, I. G., C. M. Trudinger, and R. J. Francey, A synthesis inversion of the concentration and $\delta^{13}C$ of atmospheric CO_2, *Tellus Ser. B., 47*, 35–52, 1995.

Fine, R. A., Tracers, time scales, and the thermohaline circulation: The lower limb in the North Atlantic ocean, *U.S. Natl. Rep. Int. Union Geod. Geophys. 1991-1994, Rev. Geophys., 33*, 1353–1365, 1995.

Gates, W., and A. Nelson, A new (revised) tabulation of the Scripps topography on a 1 degree global grid, technical rep., Part II, ocean depths, Rand Corp., Santa Monica, Calif.,1975.

Goyet, C., and P. G. Brewer, Biochemical properties of the oceanic carbon cycle, in *Modeling Oceanic Climate Interactions*, edited by J. Willebrand and D. L. T. Anderson, pp. 271–297, Springer-Verlag, New York, 1993.

Goyet, C., and A. Poisson, New determination of carbonic acid dissociation constants in seawater as a function of temperature and salinity, *Deep Sea Res., 36*(11), 2635–1654, 1989.

Jenkins, W. J., ^3H and ^3He in the Beta Triangle: Observations of gyre ventilation and oxygen utilization rates, *J. Phys. Oceanogr., 17*, 763–783, 1987.

Jenkins, W. J., and J. C. Goldman, Seasonal oxygen cycling and primary production in the Sargasso Sea, *J. Mar. Res., 43*, 465–491, 1985.

Kawase, M., and J. L. Sarmiento, Nutrients in the Atlantic thermocline, *J. Geophys. Res., 90*(C5), 8961–8979, 1985.

Kawase, M., and J. L. Sarmiento, Circulation and nutrients in middepth Atlantic waters, *J. Geophys. Res., 91*(C8), 9749–9770, 1986.

Keeling, C. D., NATO lecture 2: Surface ocean CO_2, in *The Global Carbon Cycle*, edited by M. Heimann, pp. 413–430, Springer-Verlag, New York, 1993.

Keeling, C. D., and T. Whorf, Atmospheric CO_2 records from sites in the SIO air sampling network, in *Trends '93: A Compendium of Data on Global Change*, edited by T. Boden, D. Kaiser, R. Sepanski, and F. Stoss, *Rep. ORNL/CDIAC-65*, pp. 16–26, Carbon Dioxide Inf. Anal. Cent., Oak Ridge Natl. Lab., Oak Ridge, Tenn., 1994.

Keeling, C. D., S. C. Piper, and M. Heimann, A three dimensional model of atmospheric CO_2 transport based on observed winds, 4, Mean annual gradients and interannual variations, in *Aspects of Climate Variability in the Pacific and the Western Americas, Geophys. Monogr. Ser., vol. 55, edited by D. H. Peterson*, pp. 305–363, AGU, Washington, D.C., 1989.

Keeling, R. F., and S. R. Shertz, Seasonal and interannual variations in atmospheric oxygen and implications for the global carbon cycle, *Nature, 358*, 723–727, 1992.

Levitus, S., and T. Boyer, *NOAA Atlas NESDIS 3: World ocean atlas 1994*, vol. 4, *Temperature*, Tech. Rep., Natl. Oceanic and Atmos. Admin., Silver Spring, Md., 1994.

Levitus, S., R. Burgett, and T. Boyer, *NOAA Atlas NESDIS 3: World ocean atlas 1994*, vol. 3, *Salinity*, Tech. Rep., Natl. Oceanic and Atmos. Admin., Silver Spring, Md., 1994.

McCartney, M., and L. Talley, The subpolar mode water of the North Atlantic Ocean, *J. Phys. Oceanogr., 12*, 1169–1188, 1982.

Millero, F. J., Thermodynamics of the carbon dioxide system in the oceans, *Geochim. Cosmochim. Acta, 59*(4), 661–677, 1995.

Minster, J., and M. Boulahdid, Redfield ratios along isopycnal surfaces - A complimentary study, *Deep Sea Res., 34*(12), 1981–2003, 1987.

Neftel, A., H. Friedli, E. Moor, H. Lötscher, H. Oeschger, U. Siegenthaler, and B. Stauffer, Historical CO_2 record from the Siple station ice core, in *Trends '93: A Compendium of Data on Global Change*, edited by T. Boden, D. Kaiser, R. Sepanski, and F. Stoss, *Rep. ORNL/CDIAC-65*, pp. 11–14, Carbon Dioxide Inf. Anal. Cent., Oak Ridge Natl. Lab., Oak Ridge, Tenn., 1994.

Oceanographic Data Facility (ODF), South Atlantic Ventilation Experiment (SAVE), *Chemical, Physical and CTD Data Report, Legs 1-3*, Scripps Inst. of Oceanogr., La Jolla, Calif., 1992a.

Oceanographic Data Facility (ODF), South Atlantic Ventilation Experiment (SAVE), *Chemical, Physical and CTD Data Report, Legs 4-5*, Scripps Inst. of Oceanogr., La Jolla, Calif., 1992b.

Peng, T.-H., and W. S. Broecker, C/P ratios in marine detritus, *Global Biogeochem. Cycles, 1*(2), 155–161, 1987.

Physical and Chemical Oceanographic Data Facility (PCODF), Transient Tracers in the Ocean: North Atlantic Study, *Shipboard Physical and Chemical Data Report*, Scripps Inst. of Oceanogr., La Jolla, Calif., 1986a.

Physical and Chemical Oceanographic Data Facility (PCODF), Transient Tracers in the Ocean: Tropical Atlantic Study, *Shipboard Physical and Chemical Data Report*, Scripps Inst. of Oceanogr., La Jolla, Calif., 1986b.

Poisson, A., and C.-T. A. Chen, Why is there so little anthropogenic CO_2 in the Antarctic Bottom Water?, *Deep Sea Res., 7*, 1255–1275, 1987.

Quay, P. D., B. Tilbrook, and C. S. Wong, Oceanic uptake of fossil fuel CO_2: Carbon-13 evidence, *Science, 256*, 74–79, 1992.

Redfield, A. C., B. H. Ketchum, and F. A. Richards, The influence of organisms on the composition of sea-water, in *The Sea*, vol. 2, edited by M. N. Hill, pp. 26–77, Wiley-Interscience, New York, 1963.

Rodriguez, J., 1993, *Beiträge zur Verteilung von ^{39}Ar im Atlantik*, Ph.D. thesis, Univ. of Bern, Bern, Switzerland.

Rooth, C., and H. Östlund, Penetration of tritium into the Atlantic thermocline, *Deep Sea Res., 19*, 481–492, 1972.

Sarmiento, J. L., and E. T. Sundquist, Revised budget for the oceanic uptake of anthropogenic carbon dioxide, *Nature, 356*, 589–593, 1992.

Sarmiento, J. L., C. G. H. Rooth, and W. Roether, The North Atlantic tritium distribution in 1972, *J. Geophys. Res., 87*(C10), 8047–8056, 1982.

Sarmiento, J. L., J. C. Orr, and U. Siegenthaler, A perturbation simulation of CO_2 uptake in an ocean general circulation model, *J. Geophys. Res., 97*(C3), 3621–3645, 1992.

Sarmiento, J. L., R. Murnane, and C. LeQuéré, Air-sea CO_2 transfer and the carbon budget of the North Atlantic, *Philos. Trans. R. Soc., London, B, 348*, 211–219, 1995.

Schimel, D., I. Enting, M. Heimann, T. Wigley, D. Raynaud, D. Alves, and U. Siegenthaler, Chapter CO_2 and the carbon cycle, in *Climate Change 94, Radiative Forcing of Climate Change*, pp. 38-71, Intergov. Panel on Clim. Change, 1994. (Available from Cambridge Univ. Press, New York.)

Schlosser, P., G. Bönisch, B. Kromer, H. Loosli, R. Bühler, R. Bayer, G. Bonani, and K. Koltermann, Mid-1980s distribution of tritium, ^3He, ^{14}C, and ^{39}Ar in the Greenland/Norwegian seas and the Nansen Basin of the Arctic Ocean, *Progr. Oceanogr., 35*, 1–28, 1995.

Shiller, A. M., Calculating the oceanic CO_2 increase: A need for caution, *J. Geophys. Res., 86*(C11), 11083–11088, 1981.

Shiller, A. M., Reply to comment by *Chen et al.*, on "Calculating the oceanic CO_2 increase: A need for caution" by A.M Shiller, *J. Geophys. Res., 87*(C3), 2086, 1982.

Shiller, A. M., and J. M. Gieskes, Processes affecting the oceanic distributions of dissolved calcium and alkalinity, *J. Geophys. Res., 85*(C5), 2719–2727, 1980.

Siegenthaler, U., and F. Joos, Use of a simple model for studying oceanic tracer distributions and the global carbon cycle, *Tellus Ser. B., 44*, 186–207, 1992.

Siegenthaler, U., and J. L. Sarmiento, Atmospheric carbon dioxide and the ocean, *Nature, 365*, 119–125, 1993.

Smethie, W., D. Chipman, J. Swift, and K. Koltermann, Chlorofluromethanes in the Arctic Mediterranean Seas: Evidence for formation of bottom water in the Eurasian Basin and deep-water exchange through Fram Strait, *Deep Sea Res., 35*, 347–369, 1988.

Stocker, T. F., W. S. Broecker, and D. G. Wright, Carbon uptake experiments with a zonally averaged global circulation model, *Tellus Ser. B., 46*, 103–122, 1994.

Swift, J., The circulation of the Denmark Strait and Iceland-Scotland overflow waters in the North Atlantic, *Deep Sea Res., 31*, 1339–1355, 1984a.

Swift, J., A recent θ-S shift in the deep waters of the northern North Atlantic, in *Climate Processes and Climate Sensitivity*, edited by J. Hansen and T. Takahashi, Geophys. Monogr. Ser., 29, pp. 39–47, AGU, Washington, D.C., 1984b.

Takahashi, T., Precision and accuracy of the GEOSECS Indian Ocean alkalinity and total CO_2 concentrations data, in *GEOSECS Indian Ocean Expedition*, edited by R. Weiss, W. Broecker, H. Craig, and D. Spencer, vol. 5, Hydrographic Data 1977-1978, pp. 5–7, U.S. Gov. Print. Off., Washington, D.C., 1983.

Takahashi, T., and P. Brewer, Hydrographic and chemistry data for the TTO/NAS expedition, April - October, 1981: Revised carbon chemistry data, letter to CDIAC, Carbon Dioxide Inf. Anal. Cent., Oak Ridge Natl. Lab., Oak Ridge, Tenn., 1986.

Takahashi, T., W. Broecker, S. Werner, and A. E. Bainbridge, Carbonate chemistry of the surface waters of the world oceans, in *Isotope Marine Chemistry*, edited by E. D. Goldberg, Y. Horibe, and K. Saruhashi, pp. 291–326, Uchida Rokakuho, Tokyo, 1980.

Takahashi, T., W. S. Broecker, and A. E. Bainbridge, The alkalinity and total carbon dioxide concentration in the world oceans, in *Scope 16: Carbon Cycle Modelling*, edited by B. Bolin, pp. 271–286, John Wiley, New York, 1981.

Takahashi, T., W. S. Broecker, and S. Langer, Redfield ratio based on chemical data from isopycnal surfaces, *J. Geophys. Res., 90*(C4), 6907–6924, 1985a.

Takahashi, T., J. Olafsson, W. S. Broecker, J. Goddard, D. W. Chipman, and J. White, Seasonal variability of the carbon-nutrient chemistry in the ocean areas west and north of Iceland, *J. Mar. Res. Inst. Reykjavik, 9*, 20–36, 1985b.

Takahashi, T., J. Olafsson, J. G. Goddard, D. W. Chipman, and S. C. Sutherland, Seasonal variation of CO_2 and nutrients in the high-latitude surface oceans: a comparative study, *Global Biogeochem. Cycles, 7*(4), 843–878, 1993.

Takahashi, T., T. T. Takahashi, and S. C. Sutherland, An assessment of the role of the North Atlantic as a CO_2 sink, *Philos. Trans. R. Soc., London, B, 348*, 143–152, 1995.

Tans, P. P., I. Y. Fung, and T. Takahashi, Observational constraints on the global atmospheric CO_2 budget, *Science, 247*, 1431–1438, 1990.

Thiele, G., and J. L. Sarmiento, Tracer dating and ocean ventilation, *J. Geophys. Res., 95*(C6), 9377–9391, 1990.

Toggweiler, J. R., K. Dixon, and K. Bryan, Simulations of radiocarbon in a coarse-resolution world ocean model, 1, steady state prebomb distributions, *J. Geophys. Res., 94*(C6), 8217–8242, 1989a.

Toggweiler, J. R., K. Dixon, and K. Bryan, Simulations of radiocarbon in a coarse-resolution world ocean model, 2, distribution of bomb-produced carbon 14, *J. Geophys. Res., 94*(C6), 8243–8264, 1989b.

Tsunogai, S., T. Ono, and S. Watanabe, Increase in total carbonate in the Western North Pacific water and a hypothesis on the missing sink of anthropogenic carbon, *J. Oceanogr., 49*, 305–315, 1993.

Veronis, G., The role of models in tracer studies, in *Numerical Models of the Ocean Circulation*, pp. 133–146, Nat. Acad. of Sci., Washington, D.C., 1975.

Volk, T., and M. I. Hoffert, Ocean carbon pumps: Analysis of relative strengths and efficiencies in ocean-driven atmospheric CO_2 changes, in *The Carbon Cycle and Atmosperic CO_2: Natural Variations Archean to Present*, Geophys. Monogr. Ser., vol. 32, edited by E. T. Sundquist and W. S. Broecker, pp. 99–110, AGU, Washington, D.C., 1985.

Wallace, D. W. R., Monitoring global ocean carbon inventories, *OOSDP Background Rep., 5, Ocean Obs. Syst. Dev. Panel*, Texas A&M Univ., College Station, Texas, 1995.

Weiss, R., Carbon dioxide in water and seawater: The solubility of non-ideal gas, *Mar. Chem., 2*, 203–215, 1974.

Weiss, R., W. Broecker, H. Craig, and D. Spencer, Hydrographic Data 1977-1978, in *GEOSECS Indian Ocean Expedition*, vol. 5, U.S. Gov. Print. Off., Washington, D.C., 1983.

Weiss, R., J. Bullister, R. Gammon, and M. Warner, Atmospheric chlorofluoromethanes in the deep equatorial Atlantic, *Nature, 314*, 608–610, 1985.

N. Gruber and T.F. Stocker, Climate and Environmental Physics, Physics Institute, University of Bern, Sidlerstr. 5, 3012 Bern, Switzerland (e-mail: gruber@climate.unibe.ch; stocker@climate.unibe.ch)

J.L. Sarmiento, Program in Atmospheric and Oceanic Sciences, Princeton University, Princeton, NJ 08544 (email: jls@splash.princeton.edu)

(Received January 19, 1996; revised April 29, 1996; accepted May 20, 1996.)